Epistatic interactions between *PHOTOPERIOD-1, CONSTANS 1* and *CONSTANS 2* modulate the photoperiodic response in wheat

Lindsay M. Shaw[1, 2]*, Chengxia Li[1, 3]*, Daniel P. Woods[1, 3]*, Maria A. Alvarez[1]*, Huiqiong Lin[1, 3], Mei Y. Lau[1], Andrew Chen[1, 4], and Jorge Dubcovsky[1, 3#]

*The first four authors contributed equally to this work

[1] Department of Plant Sciences, University of California, Davis, CA 95616. U.S.A.

[2] Currently at Queensland Alliance for Agriculture and Food Innovation, The University of Queensland, Brisbane, QLD 4072, Australia

[3] Howard Hughes Medical Institute, Chevy Chase, MD 20815, U.S.A.

[4] Currently at School of Agriculture and Food Science, The University of Queensland, St Lucia, QLD, 4067, Australia.

Lindsay Shaw: ORCID 0000-0001-8078-2409
Chengxia Li: ORCID 0000-0003-4634-8451
Maria Alejandra Alvarez: ORCID 0000-0003-2916-4255
Daniel P. Woods: ORCID 0000-0002-1498-5707
Jorge Dubcovsky: ORCID 0000-0002-7571-4345

Short title: Regulation of wheat heading time by photoperiod

Corresponding authors: Jorge Dubcovsky, Email: jdubcovsky@ucdavis.edu, Phone: 530 (752)-5159.

Abstract

In Arabidopsis, *CONSTANS* (*CO*) integrates light and circadian clock signals to promote flowering under long days (LD). In the grasses, a duplication generated two paralogs designated as *CONSTANS 1* (*CO1*) and *CONSTANS 2* (*CO2*). Here we show that in tetraploid wheat plants grown under LD, combined loss-of-function mutations in the A and B-genome homeologs of *CO1* and *CO2* (*co1 co2*) result in a small (3 d) but significant (P<0.0001) acceleration of heading time both in *PHOTOPERIOD1* (*PPD1*) sensitive (*Ppd-A1b*, functional ancestral allele) and insensitive (*Ppd-A1a*, functional dominant allele) backgrounds. Under short days (SD), *co1 co2* mutants headed 13 d earlier than the wild type (P<0.0001) in the presence of *Ppd-A1a*. However, in the presence of *Ppd-A1b*, spikes from both genotypes failed to emerge by 180 d. These results indicate that *CO1* and *CO2* operate mainly as weak heading time repressors in both LD and SD. By contrast, in *ppd1* mutants with loss-of-function mutations in both *PPD1* homeologs, the wild type *Co1* allele accelerated heading time >60 d relative to the *co1* mutant allele under LD. We detected significant genetic interactions among *CO1*, *CO2* and *PPD1* genes on heading time, which were reflected in complex interactions at the transcriptional and protein levels. Loss-of-function mutations in *PPD1* delayed heading more than combined *co1 co2* mutations and, more importantly, *PPD1* was able to perceive and respond to differences in photoperiod in the absence of functional *CO1* and *CO2* genes. Similarly, *CO1* was able to accelerate heading time in response to LD in the absence of a functional *PPD1*. Taken together, these results indicate that *PPD1* and *CO1* are able to respond to photoperiod in the absence of each other, and that interactions between these two photoperiod pathways at the transcriptional and protein levels are important to fine-tune the flowering response in wheat.

Author summary

An understanding of the mechanisms involved in the regulation of wheat heading time is required to engineer more productive varieties better adapted to new or changing environments. A large proportion of wheat's natural variation in heading time is determined by differences in genes controlling the photoperiodic response. In this study, we show that the wheat *PHOTOPERIOD1* (*PPD1*) gene has a stronger effect on heading time than *CONSTANS1* (*CO1*) and *CO2* in the regulation of the photoperiodic response, and that complex genetic interactions among these genes are important to fine-tune heading time. Using loss-of-function mutants for both *CO1* and *CO2*, we demonstrate that these genes are not required for *PPD1* to perceive differences in photoperiod and regulate heading time. Similarly, we show that in the absence of *PPD1*, *CO1* can accelerate heading time more than 60 days in response to long days. Our results indicate that each of these two wheat photoperiod pathways can respond to differences in photoperiod even in the absence of the other one. Differences in the relative importance of these two pathways and in their epistatic interactions have contributed to the diversity of photoperiodic responses observed in different grass species.

68 **Introduction**

69 A precise adjustment of flowering time to optimal environmental conditions is critical to
70 maximize plant reproductive success. Plants have evolved complex regulatory mechanisms to
71 adjust flowering initiation in response to seasonal changes and other environmental cues. Many
72 plants, including the temperate cereals, require exposure to extended periods of cold
73 (vernalization) to gain competence to flower [1]. After their vernalization requirement has been
74 fulfilled, many plants still require inductive photoperiods to accelerate flowering. Based on their
75 light requirements for floral induction, plants can be classified into long day (LD), short day
76 (SD) or day-neutral plants [2].

77 The regulatory pathway that controls flowering in response to photoperiod is best characterized
78 in the model plant *Arabidopsis thaliana*, a long day plant that flowers earlier when the days are
79 longer than a critical threshold. In this species, the external coincidence model explains the
80 integration of light signals with the circadian clock. The clock determines diurnal oscillations of
81 the gene *CONSTANS* (*CO*), which results in the coincidence of the expression peak with the light
82 phase under LD and with the dark phase under SD. Light stabilizes the CO protein, resulting in
83 the induction of *FLOWERING LOCUS T* (*FT*) and the promotion of flowering under LD. Under
84 SD, the degradation of the CO protein in the dark prevents the activation of *FT* [3-5]. Thus, *co*
85 mutants in Arabidopsis flower later than wild type under LD but at the same time as wild type
86 under SD [6].

87 CO belongs to a family of transcription factors characterized by two zinc finger B-Box domains
88 at the N-terminus and by a CONSTANS, CONSTANS-like, TIMING OF CAB EXPRESSION 1
89 (CCT) domain at the C-terminus, a structure conserved in Arabidopsis and the grass homologs
90 [7]. The *Oryza sativa* (rice) genome contains a single *CO* gene designated as *Hd1* [8], whereas

91 two paralogs designated as *CO1* and *CO2* have been identified in *Brachypodium distachyon*,
92 barley and wheat [9]. In the last three species, the predicted CO1 protein lacks conserved
93 cysteine residues at the start of the second B-box, suggesting a modified or non-functional B-box
94 2 in the temperate grasses [7, 9]. Phylogenetic and comparative genomics analyses suggest that
95 *CO1* and *CO2* paralogs originated by a segmental duplication at the base of the grass family,
96 with *CO1* located in the ancestral position colinear with rice *Hd1,* whereas *CO2* was lost in rice
97 and is likely not functional in sorghum [9]

98 Overexpression of *CO1* and *CO2* under the maize *UBIQUITIN* promoter in spring barley,
99 promoted flowering under both LD and SD conditions by upregulating *FT1* [10, 11]. However,
100 both *Ubi::CO1* and *Ubi::CO2* transgenic lines flowered 42-43 d later in SD than in LD
101 indicating the existence of additional genes controlling the photoperiodic response [10, 11]. In
102 barley, the response to photoperiod is determined mainly by the pseudo-response regulator gene
103 *PHOTOPERIOD1* (*PPD1*) [12], also known as *PRR37* in rice [13] and *Sorghum bicolor*
104 (sorghum) [14]. This gene is regulated by the circadian clock and the phytochrome-mediated
105 light signaling pathway and encodes a protein with a pseudo-receiver domain and a CCT domain
106 [14, 15].

107 In wheat, natural deletions in the promoter region of *PPD-A1* (*Ppd-A1a* allele) and *PPD-D1*
108 (*Ppd-D1a* allele) are associated with increased transcript levels and accelerated heading under
109 SD relative to the ancestral *Ppd1b* allele [16, 17]. As a result, plants carrying the *Ppd1a* alleles
110 show reduced differences in heading time between LD and SD and are designated as photoperiod
111 insensitive (PI), whereas plants carrying the *Ppd1b* allele are designated as photoperiod sensitive
112 (PS) [16, 17]. However, wheat PI lines still exhibit a significant acceleration of flowering under

113 LD relative to SD and, therefore, the wheat PI designation is used in this study to indicate a
114 reduced photoperiodic response rather than a lack of a photoperiodic response.

115 Under LD conditions, the wheat *PPD1* gene induces the expression of *FT1*, which encodes a
116 mobile protein that travels to the shoot apical meristem (SAM), where it promotes the expression
117 of the floral homeotic MADS box transcription factor *VERNALIZATION1* (*VRN1*) and the
118 synthesis of gibberellic acid (GA) [18]. The simultaneous presence of GA and *VRN1* results in
119 the up-regulation of *SUPPRESSOR OF OVEREXPRESSION OF CONSTANS1-1* (*SOC1*) and
120 *LEAFY* (*LFY*) genes, which are required for normal and timely spike development, stem
121 elongation and spike emergence or heading [18]. In photoperiod sensitive wheats grown under
122 SD, the SAM transitions to the reproductive stage, but stem elongation and spike development
123 proceed very slowly and heads fail to emerge or emerge extremely late [19]. These results
124 indicate that in wheat, the photoperiod pathway has a larger impact on the duration of spike
125 development and stem elongation than on the initial transition between the vegetative and
126 reproductive stages [18, 19]. The addition of gibberellic acid (GA) to PS spring wheat grown
127 under SD accelerates spike development, but only in lines that express *VRN1* under SD [18].

128 The photoperiod and vernalization pathways converge at the regulation of *FT1* in the leaves. The
129 role of *PPD1* as a LD flowering promoter is antagonized in winter wheats by the role of *VRN2* as
130 a LD flowering repressor [20, 21], which prevents the induction of *FT1* during the fall. Long
131 exposures to cold temperatures during the winter (vernalization) result in the induction of *VRN1*
132 both in the leaves and in the SAM [22]. In the leaves, the presence of *VRN1* prevents the
133 upregulation of *VRN2* in the spring [23], which results in the upregulation of *FT1* under LD. In
134 the SAM, the upregulation of *VRN1* initiates the transition of the SAM to the reproductive phase,
135 but spike development proceeds slowly until the LD induction of *FT1*. The arrival of *FT1* to the

136 SAM further up-regulates *VRN1* and induces GA accumulation, which results in accelerated
137 spike development and stem elongation [18].

138 In addition to the natural *PPD1* alleles (PS and PI), induced loss-of-function mutations in all
139 *PPD1* homeologs (henceforth, *ppd1*) have been developed for both hexaploid [24] and tetraploid
140 wheat [19]. These *ppd1* plants show large delays in spike development and heading time under
141 LD, and spikes usually emerge very late, fail to emerge or are aborted under SD [19, 24]. The
142 flowering phenotypes of the wheat *ppd1* mutants are more drastic than those described for the
143 barley photoperiod insensitive allele *ppd-H1*, which has only amino acid changes and is likely a
144 hypomorphic allele rather than a complete loss-of-function allele [12]. It is important to
145 differentiate the photoperiod insensitive allele in barley that refers to delayed heading under LD,
146 from the PI allele in wheat that refers to accelerated flowering under SD.

147 *CO1* and *CO2* overexpression results in barley suggest a role of these genes as flowering
148 promoters [10, 11]. However, overexpression under a constitutive promoter results in elevated
149 transcript levels and ectopic expression in tissues or developmental phases that are different from
150 those of the natural alleles, which complicates the interpretation of results. The use of loss-of-
151 function mutations can provide a better understanding of the role of these genes under more
152 natural conditions. In this study, we investigate the role of *CO1* and *CO2* on the photoperiod
153 response in wheat using loss-of-function mutants for both genes in the tetraploid spring wheat
154 variety Kronos. In addition, we combine loss-of-function mutations in *co1*, *co2* and *ppd1* to
155 study the effect of their genetic interactions on heading time and on the transcription profiles of
156 critical flowering genes. We also investigate the interactions among the proteins encoded by
157 these genes. Taken together, these analyses show complex genetic interactions among *CO1*, *CO2*

158 and *PPD1* on heading time that reflect similarly complex interactions at the transcriptional and
159 protein levels.

160

161 **Results**

162 **Identification of *CO1* and *CO2* loss-of-function mutants in wheat**

163 We identified a total of 153 mutations in the A and B homeologs of *CO1* and *CO2* in the Kronos
164 tetraploid TILLING population [25, 26] using primers and PCR conditions listed in Supporting
165 Information Table S1. Among the 153 mutations, 74 resulted in non-synonymous amino acid
166 changes, and five introduced early stop codons resulting in truncated non-functional proteins
167 (Table S2). These five truncation mutations were validated by sequencing and one for each
168 homeolog was selected to study the function of *CO1* and *CO2* (Fig 1). We backcrossed the
169 individual mutant lines with wild-type Kronos at least twice to reduce background mutations.

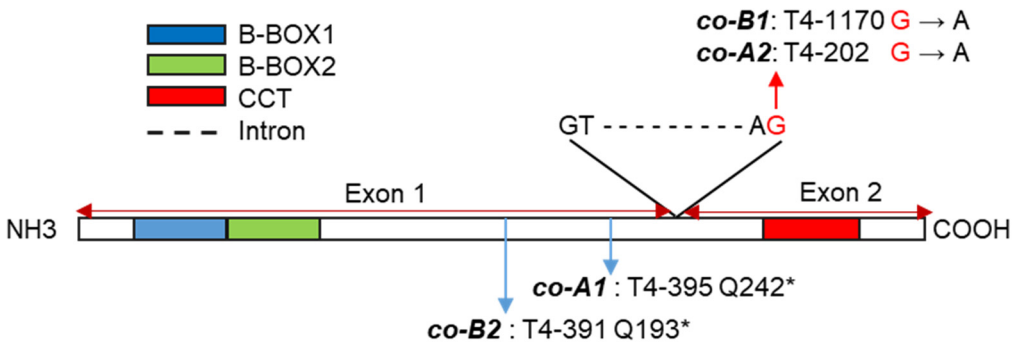

170

171 **Fig 1: *CO1* and *CO2* gene structure and position of the selected TILLING mutations.** Both *CO1* and
172 *CO2* genes have two exons, which encode two B-BOX domains at the N-terminus and a CCT domain at
173 the C-terminus. The selected *co-A1* and *co-B2* mutations, located in the first exon after the two B-Box
174 domains, are predicted to generate premature stop codons, whereas the *co-B1* and *co-A2* mutants have
175 acceptor splice-site mutations that result in intron retention and premature stop codons that eliminate the
176 complete exon 2 including the CCT domain. The T4 numbers are the mutant identification. The schematic
177 gene structure is based on *CO-A1* from Kronos (GenBank MT043302).

178 We generated a *co1* loss-of-function mutant by crossing *co-A1* mutant T4-395 (Q242*) with *co-*
179 *B1* mutant T4-1170 (Exon2 acceptor splice site mutation). To generate the *co2* loss-of-function
180 mutant, we crossed *co-A2* mutant T4-202 (Exon 2 acceptor splice site mutation) with *co-B2*
181 mutant T4-391 (Q193*). Finally, we crossed the *co1* and *co2* mutants and generated a *co1 co2*
182 double mutant. The stop codon mutations in *co-A1* and *co-B2* truncate the carboxyl terminal half
183 of the CONSTANS protein including the CCT domain (Fig 1), which is critical for protein
184 function in both Arabidopsis and cereals [27]. Likewise, the splice-site mutations selected in the
185 *co-B1* and *co-A2* mutants result in intron retention and premature stop codons that also eliminate
186 the conserved CCT domain. Based on these large truncations we concluded that *co1 co2* has
187 loss-of-function mutations for all *CO1* and *CO2* homeologs.

188

189 **Effect of *PPD1* photoperiod sensitive (PS) and insensitive (PI) alleles on heading time and**
190 **spike development**

191 We transferred the four *co1 co2* mutations generated in Kronos-PI into a near-isogenic Kronos-
192 PS line [18] to study the effect of these mutations in two different backgrounds with large
193 differences in heading time under SD. To establish a baseline for comparison, we first describe
194 the effect of the two *PPD1* alleles in lines carrying the wild type *Co1* and *Co2* alleles (Fig 2A,
195 blue bars).

196 Under LD, heading time was 2.5 d earlier in Kronos-PI (52.3 ± 0.4 d) than in Kronos-PS (54.8 ±
197 0.3 d). Although the difference was small, it was highly significant ($P < 0.0001$) and consistent
198 with previously published results [15]. Under SD, the differences between the two genotypes
199 were much larger (>66 d, $P < 0.0001$), with Kronos-PI heading at 113.2 ± 0.4 d and Kronos-PS
200 spikes failing to emerge before the experiment was terminated at 180 d. The earlier flowering of

201 Kronos-PI under SD reduced the difference between SD and LD in this genotype (61 d) relative

202 to Kronos-PS (>125 d, Fig 2A blue bars).

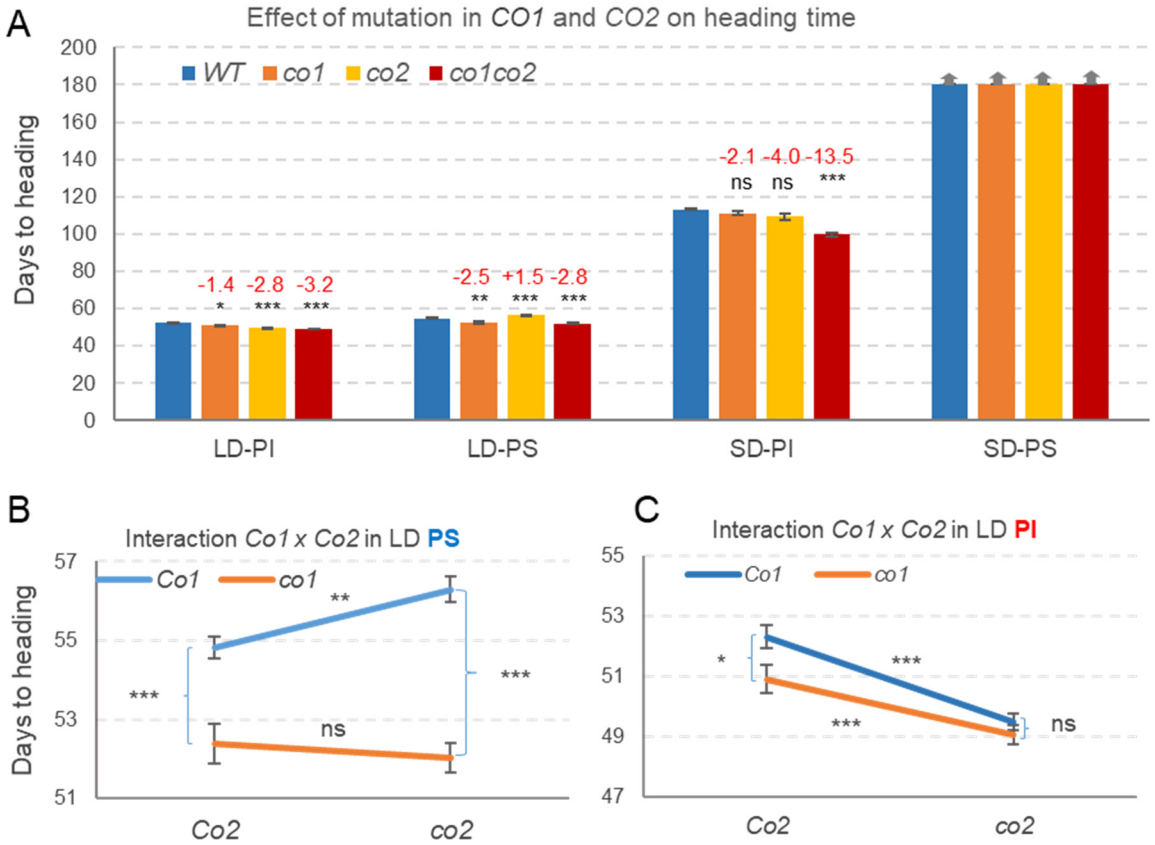

203

204 **Fig. 2: Heading time of wild type, *co1, co2* and *co1 co2* mutants under LD and SD in Kronos-PI**

205 **(*Ppd-A1a*) and Kronos-PS (*Ppd-A1b*) backgrounds**. (**A**) Averages are based on 15-19 plants in LD-PI

206 (2 experiments), 21-24 plants in LD-PS (3 experiments) and 8 to 14 plants in SD-PI and SD-PS (1

207 experiment). Red numbers indicate differences in heading time relative to the wild type (mut-WT), with *P*

208 values from a Dunnett test. Vertical arrows above the bars indicate that spikes have not emerged at 180 d

209 (end of the experiment). (**B-C**) Interaction graphs for *CO1* and *CO2* in Kronos-PS (*Ppd-A1b*) and Kronos-

210 PI (*Ppd-A1a*) backgrounds. The interaction was significant in B ($P = 0.0052$) but not in C (Table S3).

211 Error bars are standard errors of the means (henceforth, s.e.m). *= $P < 0.05$, **= $P < 0.01$, ***= $P <$

212 0.001, ns= not significant.

213

214 To determine if the observed differences in heading time were the result of changes in the
215 duration of the vegetative phase or the spike development and elongation phases, we dissected
216 SAMs of the main tillers from the different genotypes (from 4- to 14-leaf stage, S1 Fig). Under
217 LD, the SAMs from both Kronos-PI and Kronos-PS reached the early stages of spike
218 development by leaf four (W3-W3.25, Waddington scale [28]), the terminal spikelet stage
219 (W3.5) by leaf six, and headed at 52-55 d (S1 Fig). Under SD, the SAMs of both genotypes were
220 at the vegetative stage by leaf four and started to elongate by leaf six. After that point, the two
221 genotypes diverged, while Kronos-PI transitioned to the terminal spikelet and lemma elongation
222 stage at the eighth leaf, Kronos-PS reached the same developmental stage at leaf 12 (S1 Fig).

223

224 **Effect of *CO1* and *CO2* on heading time in the presence of functional *PPD1* alleles**

225 Loss of *CO1* and *CO2* function resulted in small but significant changes in heading time. The
226 *co1 co2* double mutant headed 3 d earlier than the wild type in both Kronos-PI and Kronos-PS (P
227 < 0.0001) under LD, and 13.5 d earlier than the wild type in Kronos-PI under SD ($P < 0.0001$,
228 Fig 2A). In the Kronos-PS background under SD, spikes failed to emerge or were aborted in
229 most of the plants by the end of the experiment at 180 d, limiting our ability to determine
230 difference on heading time between the *co1* and *co2* mutant and wild type alleles under this
231 condition.

232 Even though the differences in heading time between *co1 co2* and wild type alleles were larger
233 under SD (13.5 d) than under LD (3 d), they were still smaller than the differences between the
234 *PPD1* photoperiod sensitive and insensitive alleles under SD (>67 d), or the differences between
235 LD and SD in Kronos-PI (61 d) or Kronos-PS (>125, Fig 2A blue bars). These results indicate

236 that, in wheat, the *PPD1* alleles have a stronger effect on the photoperiodic response than the
237 *CO1* and *CO2* genes.

238 Except for the *co2* mutant that headed later than the wild type in the Kronos-PS background
239 under LD (+1.5 d, $P < 0.0001$), all the other *co1* and *co2* single and double mutants headed
240 significantly earlier than their respective wild type controls under both LD and SD (Fig 2A).
241 These results suggest that under the tested conditions, *CO1* functions as a mild heading time
242 repressor in all backgrounds, and *CO2* as a mild heading time promoter or repressor depending
243 on the *PPD1* and *CO1* alleles present and the photoperiod (Fig 2A).

244 *Long day experiments*

245 To explore the interactions between *PPD1*, *CO1* and *CO2* under LD, we performed a factorial
246 ANOVA combining data from three experiments in Kronos-PS and two in Kronos-PI, using
247 experiments as blocks (nested within genotypes). This analysis showed highly significant effects
248 on heading time for *PPD1* ($P < 0.0001$), *CO1* ($P < 0.0001$) and *CO2* ($P = 0.0004$) and highly
249 significant two-way interactions for *PPD1* x *CO1* and *PPD1* x *CO2* ($P < 0.0001$, Table S3A).
250 The *CO1* x *CO2* interaction was not significant ($P = 0.3437$) but the three-way interaction was
251 significant ($P = 0.0046$, Table S3A), suggesting the possibility of different *CO1* x *CO2*
252 interactions in the different *PPD1* backgrounds that cancelled each other in the combined
253 analysis.

254 To test this possibility, we performed separate *CO1* x *CO2* factorial ANOVAs for Kronos-PS
255 and Kronos-PI. In the Kronos-PS background, *CO1* showed a stronger effect ($P < 0.0001$) on
256 heading time than *CO2* ($P = 0.1448$) and their interaction was significant ($P =0.0052$, Fig 2B,
257 Table S3B). By contrast, in the Kronos-PI background, *CO2* showed a stronger effect ($P <$
258 0.0001) than *CO1* ($P = 0.0157$) and the interaction was not significant. ($P = 0.1934$, Fig 2C,

259 Table S3C). In summary, these results indicate complex genetic interactions between *PPD1*,
260 *CO1* and *CO2* in the regulation of heading time under LD.

261 *Short day experiments*

262 Under SD, the Kronos-PS lines failed to flower before the experiment was terminated (180 d), so
263 we were only able to study the interactions between *CO1* and *CO2* in the Kronos-PI background.
264 All four genotypes headed between 100 and 113 d, which is 51 to 61 d later than the same lines
265 under LD. A factorial ANOVA for heading time showed significant effects for both *CO1* and
266 *CO2* ($P < 0.0001$) and a significant interaction between the two ($P = 0.0029$, Table S4). This
267 interaction was associated with the larger acceleration of heading time in the double mutant (13.5
268 d) than in the single *co1* (2.1 d) and *co2* (4.0 d) mutants (Fig 2A). This result indicates a stronger
269 effect of each mutation in the presence of the mutant allele of the other gene than in the presence
270 of the wild type allele (Table S4).

271 To see if the *co1* and *co2* mutations in the Kronos-PS background were associated with delays in
272 SAM differentiation or in spike development, we dissected apices for three plants from each
273 genotype every week from 4 to 11 weeks, and included wild type Kronos-PI as a control. Under
274 SD, all five genotypes reached the double-ridge stage (W2.5) by week 6 (Fig 3A-B). From there,
275 the Kronos-PI genotype developed more rapidly than the four Kronos-PS genotypes, which
276 showed similar developmental rates in the wild type and the *co1* and *co2* mutants (Fig 3B). By
277 week 11, the developing spikes in the Kronos-PI control were 3-13 cm long including awns, the
278 peduncles were 5 to 14 mm long, and the developing flowers were at the elongated stigmatic
279 branches stage (>W7.5). By contrast, all four Kronos-PS lines at the same time point showed no
280 peduncle elongation, produced spikes of less than 0.5 cm, and the flowers still had the stylar
281 canal open (<W6.0). These results indicate that the *co1* and *co2* mutations have a limited effect

on spike development and elongation in the Kronos-PS background under SD compared with the strong effect of the *Ppd-A1a* in Kronos-PI.

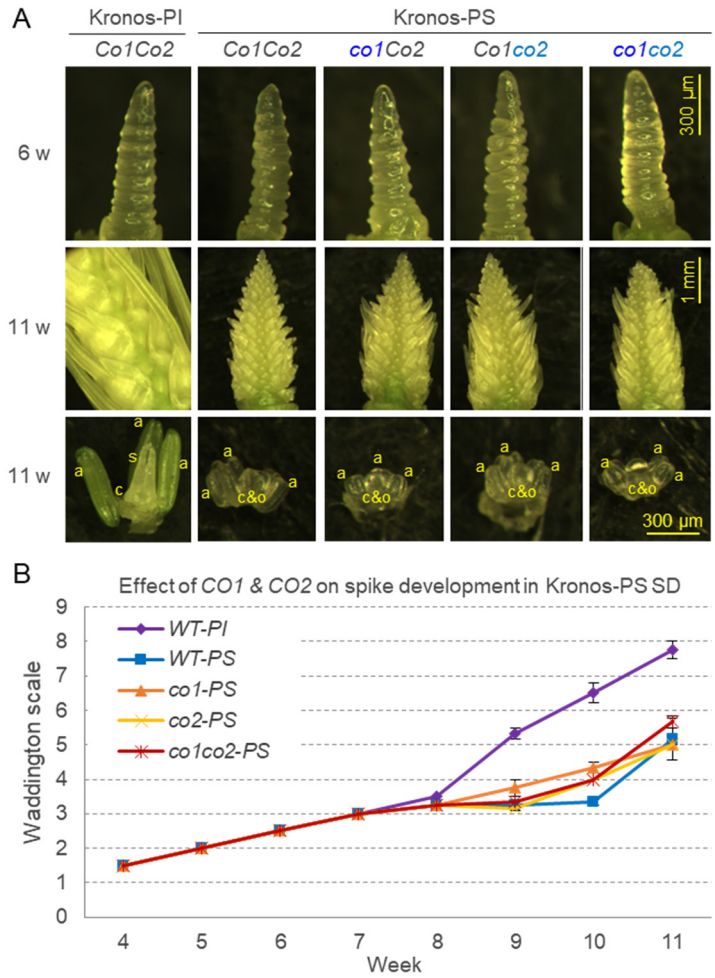

Fig 3. Effect of *co1* and *co2* mutations on spike development in Kronos-PS under SD. Kronos-PI was included as control. (**A**) Dissecting microscope images of developing apices at week 6 (double-ridge, W2.5) and week 11 with a detail of their floral organs. a = anthers, elongated in Kronos-PI and primordia in other genotypes, c = carpel and s = styles well developed in Kronos-PI and c&o = carpel extending around the ovule in other genotypes (**B**) Developmental time course of SAM using the Waddington scale from 4- through 11-week-old plants (n = 3). W1 = vegetative apex, W2 = double ridge, W3 = glume primordium, W4 = stamen primordium, W5 = carpel extending round three sides of ovule, W6 = short

292 style primordia and stylar canal open, W7 = stigmatic branches just differentiating as swollen cells on
293 styles, W8 = stigmatic branches elongating, W9 = styles and stigmatic branches erect and stigmatic hairs
294 differentiating.

295

296 **Effect of *CO1* and *CO2* on heading time in the absence of functional *PPD1* alleles**

297 To investigate the effect of *CO1* and *CO2* in the absence of *PPD1*, we introgressed the *co1* and
298 *co2* mutations into a Kronos line with loss-of-function mutations in both *PPD-A1* and *PPD-B1*
299 (*ppd1*) [19]. As before, we describe first the differences in SAM development and heading time
300 between Kronos-PS and *ppd1* mutants carrying the wild type *Co1* and *Co2* alleles to establish a
301 baseline for comparison (Fig 4A, blue bars).

302 Under LD, the plants with the *ppd1 Co1 Co2* allele combination headed much later (115.5 ± 15.3
303 d) than the Kronos-PS controls carrying the functional *Ppd1b* allele (52.5 ± 0.7 d, Fig 4A),
304 similar to results reported before [19]. The *ppd1* mutant plants showed a 79% reduction in
305 number of grains per spike relative to the Kronos-PS lines (Fig 4B-C). Apex dissections showed
306 a delayed transition to the double-ridge stage in the *ppd1* mutant (leaf 8 to 10) relative to
307 Kronos-PS (<leaf 4, S1 Fig). Similarly, the terminal spikelet was formed in Kronos-PS by leaf 6
308 but was not formed in *ppd1* by leaf 14, when the experiment was terminated (S1 Fig). Under SD,
309 spikes of both the *ppd1* mutant and Kronos-PS failed to emerge by 180 d. Dissection of the main
310 tillers from these plants showed that spike development in *ppd1* lagged behind that of Kronos-PS
311 (S1 Fig, leaf 12 and 14 and S2 Fig). These results indicate that *PPD1* is not essential for the
312 initial transition of the SAM to the reproductive stage, but in its absence, spike development and
313 stem elongation are severely compromised.

314

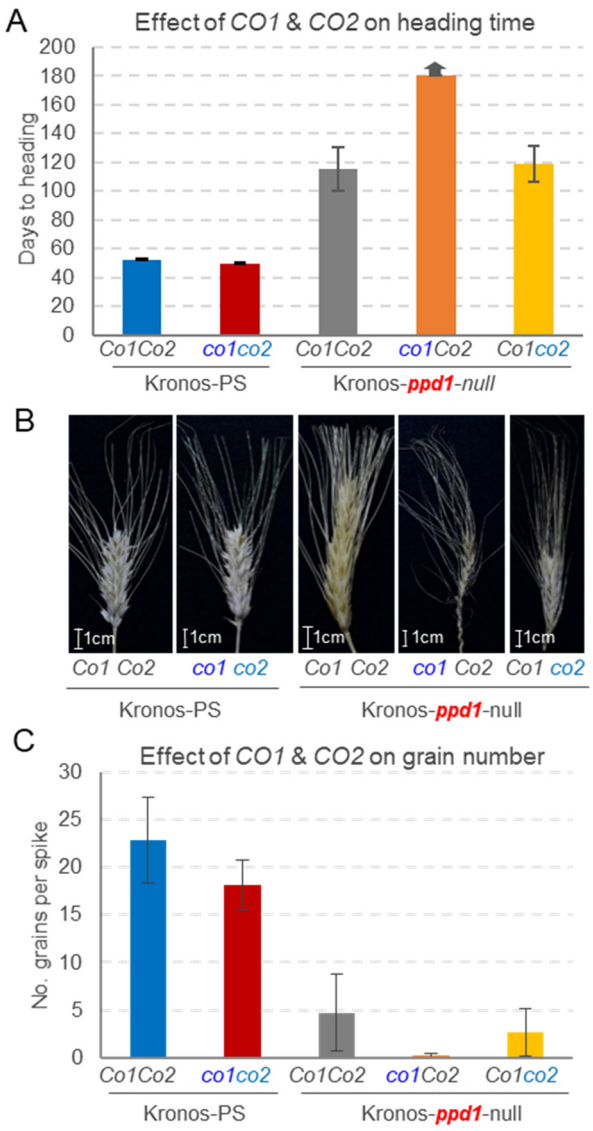

Fig 4. Phenotypic effects of *co1* and *co2* mutations in the absence of functional *PPD1* genes under LD (**A**) Average days to heading in *ppd1* mutants carrying mutations in either *co1* or *co2*. Kronos-PS wild type and *co1 co2* double mutants are included as controls. Floral transition and spike formation occurred in all genotypes, but in the *ppd1 co1* double mutant floral development was delayed or arrested and spikes failed to emerge before the experiment was terminated (arrow on top of the bar indicates heading time > 180 d) (**C**) Number of grains per spike recovered from the same genotypes as in A. Error bars are standard errors of the means calculated from 7 to 16 plants per genotype for flowering and from 4 to 8 plants for grain number.

325 The introgression of the *co2* mutation in the *ppd1* background had a limited effect on heading
326 time. Heading time of the double mutant *ppd1 co2* (119.1 ± 12.5 d) was only four days later than
327 *ppd1*, and the differences were not significant suggesting a limited effect of *CO2* on heading
328 time in the absence of a functional *PPD1*. The *ppd1 co2* double mutant showed an even more
329 severe reduction in grain production than the *ppd1* mutant (89% reduction relative to Kronos-
330 PS), but the differences were not significant.

331 The most important result was observed when we combined the *ppd1* and *co1* mutations. The
332 spikes from the *ppd1 co1* plants failed to emerge before the experiment was terminated at 180 d
333 (Fig 4A), and failed to produce any grains (Fig 4B-C). Even though we were not able to recover
334 the triple *ppd1 co1 co2* mutant, the delayed heading time of the *ppd1 co1* mutant relative to the
335 *ppd1* and *ppd1 co2* mutants (>60d) is sufficient to conclude that *CO1* can accelerate heading
336 time in response to LD even in the absence of functional *PPD1* alleles.

337

338 **Effect of mutations in *PPD1*, *CO1* and *CO2* on the transcriptional profiles of flowering**
339 **genes**

340 To better understand the regulatory networks underlying the genetic interactions described
341 above, we characterized the effect of loss-of-function mutations in *PPD1, CO1* and *CO2* on the
342 transcription profiles of several flowering genes under LD and SD. Since Kronos-PI and Kronos-
343 PS have very similar heading times under LD but not under SD, we included both genotypes in
344 the SD experiment but only Kronos-PS under LD. To perform this experiment with a
345 manageable number of plants, we included the *co1 co2* double mutants in both experiments but
346 the individual *co1* and *co2* mutants only in the LD experiment We grew the plants in a growth

347 chamber under LD or SD and sampled the fully expanded fourth leaf every 4 hours throughout a
348 24-h period.

349 Under LD, *CO1* transcripts were significantly upregulated in both *co2* and *ppd1* mutants 12
350 hours after the start of the light phase (Zeitgeber time 12 or ZT12, Fig 5A), suggesting that these
351 two genes act as transcriptional repressors of *CO1*. The negative effect of *PPD1* on *CO1*
352 transcription was also observed in a separate experiment using older plants (six-week-old). In
353 leaf samples collected at ZT4 we observed a significant upregulation of *CO1* in the *ppd1* and
354 *ppd1 co2* mutants relative to Kronos-PS (S3A Fig). No differences were detected between the
355 *ppd1* and *ppd1 co2* mutants, which suggests that the loss of *co2* function did not affect *CO1*
356 expression in the absence of functional *PPD1* genes (S3A Fig). Under SD, *CO1* transcripts
357 showed a very different profile than under LD, with a major peak in the middle of the night
358 (ZT16) in Kronos-PS and at the end of the day (ZT8) in Kronos-PI, and a different profile in the
359 *ppd1* mutant. These results indicate significant effects of *PPD1* on *CO1* transcription under both
360 LD and SD (Fig 5A).

361 Transcript levels of *CO2* were very low compared with *CO1* both under LD and SD, and showed
362 no significant differences among most genotypes (Fig 5B). We further confirmed these
363 observations in six-week old plants of Kronos-PS, *ppd1* and *ppd1 co1* plants sampled at ZT4 in
364 LD (S3B Fig).

365

366

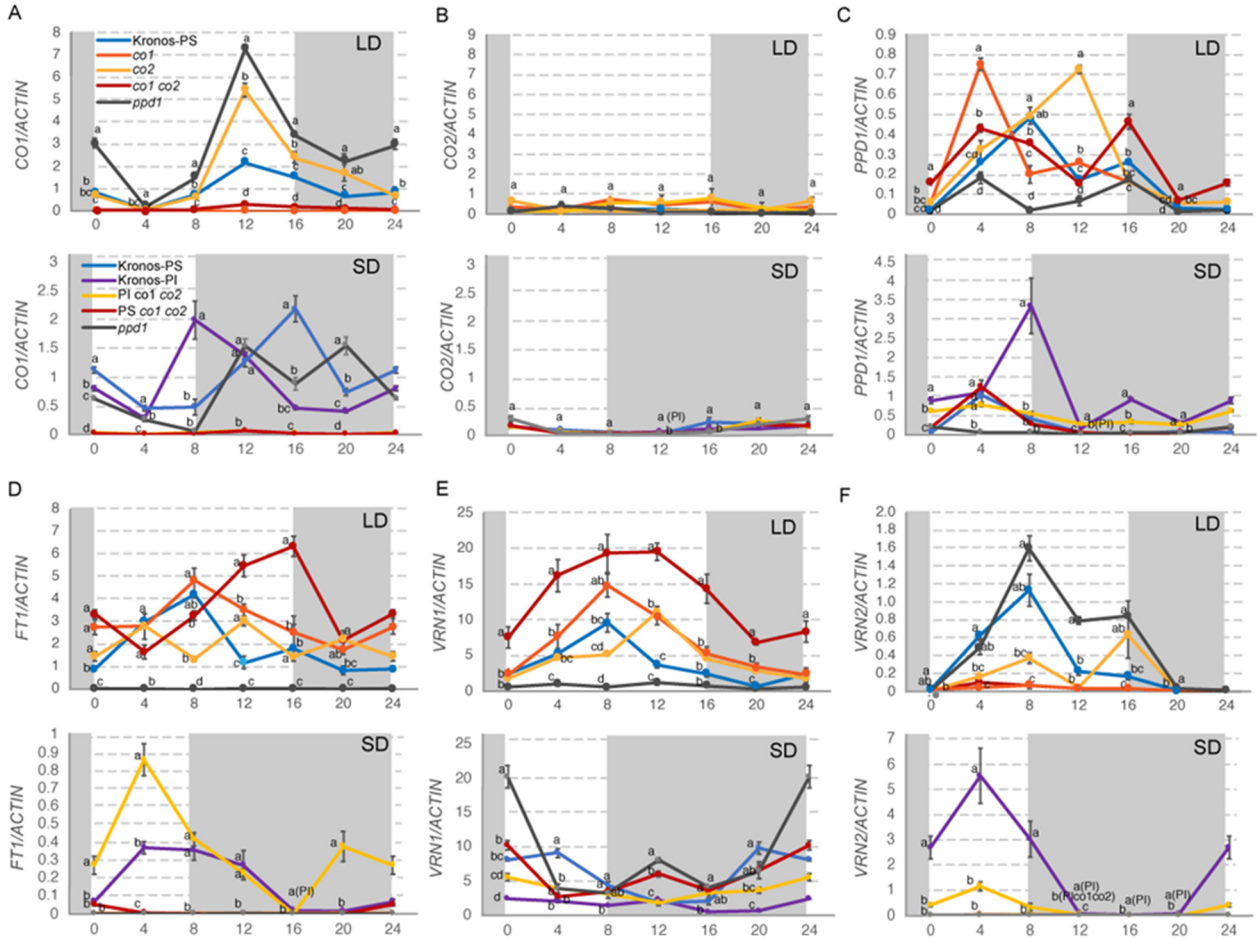

Fig 5. Effect of loss-of-function mutations in *CO1*, *CO2* and *PPD1* on the transcriptional profiles of six wheat flowering genes in Kronos-PS and Kronos-PI (SD-only) plants grown under LD and SD. (**A**) *CO1*, (**B**) *CO2*, (**C**) *PPD1*, (**D**) *FT1*, (**E**) *VRN1*, and (**F**) *VRN2.* LD experiments included Kronos-PS, *co1*, *co2*, *co1 co2*, and *ppd1* mutants; whereas SD experiments included Kronos-PS, Kronos-PI, and their respective *co1 co2* and *ppd1* mutants. We grew the plants in a growth chamber under 16 h light at 22 °C and 8 h darkness at 17 °C for LD, and under 8 h light and 16 h darkness for SD (same temperatures). Fully expanded 4th leaves (Zadoks scale =14) were harvested at ZT0, ZT4, ZT8, ZT12, ZR16, and ZT20. The ZT0 value is the same as at ZT24. Shaded boxes represent night. Values are averages of four biological replicates and bars are SE of the means. Expression values are relative to *ACTIN* using the delta Ct method. Primers and primer efficiencies are listed in Table S5 (all amplify both A and B homologs of the respective genes).

380 Under LD, the *PPD1* gene in Kronos-PS showed a main peak in the middle of the light period
381 (ZT8) and a secondary peak at dusk (ZT16), which is consistent with the *PPD1* profile
382 previously described in photoperiod sensitive *T. monococcum* [29]. In the *co1* and *co1 co2*
383 mutants, the main peak was shifted 4 h earlier (ZT4), whereas in the *co2* mutants the main peak
384 was delayed 4 h (ZT12, Fig 5C). The ZT16 peak was significantly higher than the wild type in
385 the *co1 co2* double mutant but not in the single mutants (Fig 5C). The complex effects of the *co1*
386 and *co2* mutations on *PPD1* transcription profiles reflect the significant two- and three-way
387 genetic interactions among these three genes on heading time described above.

388 Under SD, the *PPD1* profiles were very different than under LD. Kronos-PS and its respective
389 *co1 co2* mutant showed similar profiles with a peak at ZT4. By contrast, Kronos-PI showed a
390 very strong peak at ZT8 that was not observed in Kronos-PI with the *co1 co2* mutations (Fig 5C).
391 In addition, Kronos-PI and Kronos-PI *co1co2* showed significantly higher *PPD1* transcript levels
392 during the night relative to the other genotypes. The differences were largest at ZT16 (middle of
393 the night), which has been shown to be the optimum time for a short pulse of light (night break)
394 to accelerate heading time in Kronos- PS under SD [19]. The upregulation of *PPD1* during the
395 night under SD is consistent with previously published results in tetraploid wheat lines carrying
396 the *Ppd-A1a* allele (PI) relative to F_8-near-isogenic sister lines carrying the *Ppd-A1b* allele (PS)
397 [17].

398 The *FT1* profiles correlated well with heading time both in LD and SD experiments. The earlier
399 heading time of Kronos-PS *co1 co2* under LD was paralleled by significantly higher transcript
400 levels of *FT1* at the end of the day than all other genotypes (Fig 5D). Under SD, *FT1* transcript
401 levels were upregulated only in Kronos-PI genotypes, which were the only ones that headed
402 under this condition (Fig 2). Between the two Kronos-PI lines, the *co1 co2* mutant showed

403 higher *FT1* transcript levels and flowered earlier (13 d, Fig 2) than the wild type (Fig 5D). We
404 observed a significant reduction of the transcript levels of *FT1* in the *ppd1* mutant relative to
405 wild type, which was also consistent with its delayed heading time under LD (Fig 4) and its
406 inability to head under SD.

407 The transcript levels of *VRN1* correlated well with the transcript levels of *FT1* under LD but not
408 under SD (Fig 5E). Under SD at dawn, *VRN1* transcript levels were higher in *ppd1* relative to the
409 other genotypes, and was generally higher in Kronos-PS than in Kronos-PI genotypes. No
410 significant differences in *VRN1* expression were detected between the *co1 co2* mutants and their
411 respective Kronos-PS and Kronos-PI isogenic lines at that time point. The Kronos-PI genotypes
412 showed limited variation during the day compared with the Kronos-PS and *ppd1* mutant (Fig.
413 5E).

414 The *VRN2* locus includes two genes, but since *ZCCT1* is not functional in tetraploid wheat [30],
415 we present only expression data for *ZCCT2*. Under LD, the transcriptional profiles of *PPD1* and
416 *ZCCT2* were similar for the wild type Kronos-PS but not for the different mutants (Fig 5). We
417 observed a small but not significant increase of *ZCCT2* transcript levels in the *ppd1* mutant and a
418 significant downregulation in the *co1* and *co1 co2* mutants. The interpretation of these results is
419 complicated by the effects of these mutations on *VRN1*, which is a known repressor of *VRN2*
420 under LD [23] (see Discussion section). Under SD, *VRN2* was upregulated only in the Kronos-PI
421 lines, with higher transcript levels in the presence of the functional *CO1 CO2* genes than in the
422 *co1 co2* mutants.

423

424

425 **Effect of *VRN1* on the transcriptional regulation of *CO1* and *CO2* under LD**

426 To explore the potential role of *VRN1* in the transcriptional regulation of *CO1* and *CO2*, we used
427 Kronos *vrn-A1* and *vrn-B1* single mutants and the *vrn-A1 vrn-B1* double mutant (henceforth
428 *vrn1*) developed previously [23]. The *vrn-B1* mutant has a functional allele of *VRN-A1* that
429 confers a dominant spring growth habit, whereas the *vrn-A1* mutant has the ancestral allele of
430 *VRN-B1* that confers a recessive winter growth habit. The *vrn1* double mutant has a delayed
431 heading time and a residual response to vernalization [23].

432 *CO1* showed significantly higher transcript levels in the late flowering *vrn-A1* and *vrn1* mutants
433 than in the rapidly flowering *vrn-B1* mutant, both in vernalized and un-vernalized plants (Fig 6
434 A-B). In all genotypes, *CO1* was downregulated to very low levels in the flag-leaf at heading
435 time. In the *vrn1* mutant, we observed a slight decrease of *CO1* transcript levels during
436 vernalization followed by a rapid upregulation when we moved the plants back to room
437 temperature (RT). By contrast, in the single *vrn-A1* and *vrn-B1* mutants, which still have one
438 functional copy of *VRN1*, *CO1* transcripts stayed low after the plants were returned to RT (Fig 6
439 A). From previous studies, we know that *VRN1* transcript levels increase slowly during LD
440 vernalization and then rapidly when plants are moved to RT and start to flower [23]. Taken
441 together, these results suggest that *VRN1* acts as a transcriptional repressor of *CO1*.

442

443

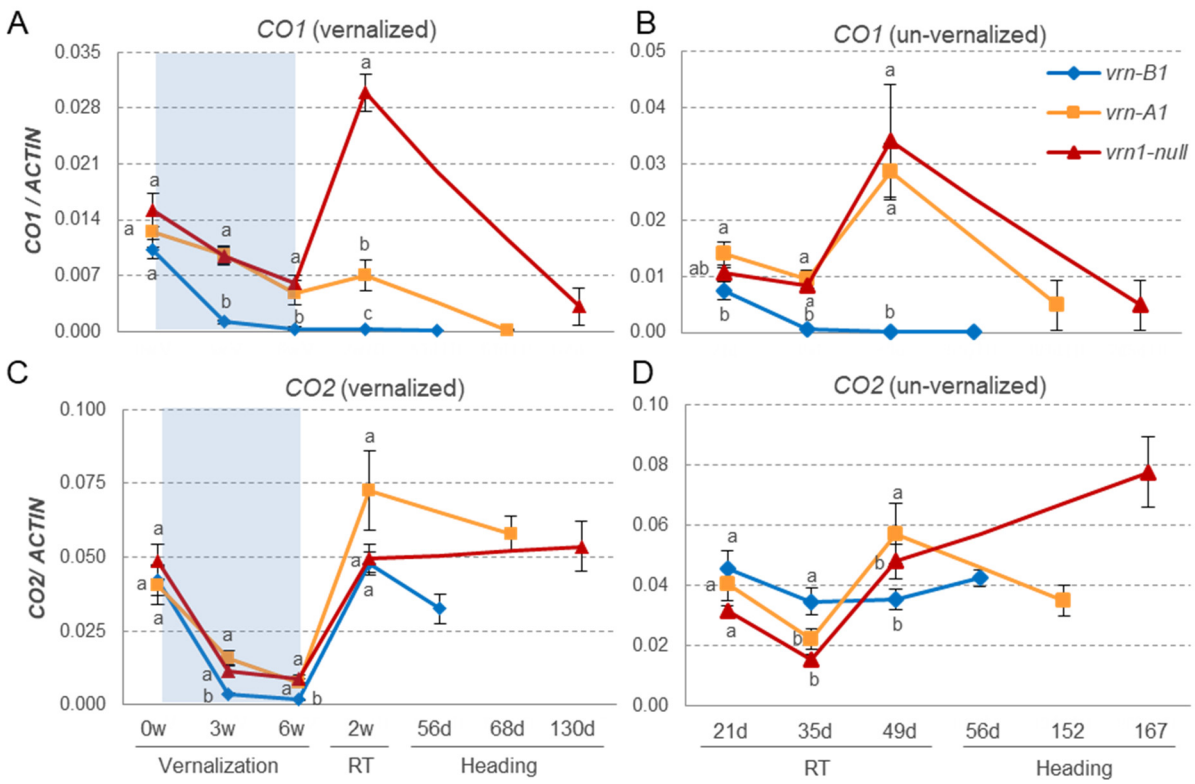

Fig 6. Effect of mutations in Kronos *vrn-A1* (winter growth habit), *vrn-B1* (spring growth habit) and *vrn-A1 vrn-B1* (*vrn1*, very late heading) on the transcriptional profiles of *CO1* and *CO2*. All mutants are homozygous and in the Kronos-PI background. (**A-B**) *CO1* and (**C-D**) *CO2* transcription profiles. **A** & **C**) More recently expanded leaves from three weeks old plants were sampled before vernalization (0w), at 3w and 6 w vernalization (4°C), 2 weeks after return to room temperature (RT= 22°C day and 18°C) and at heading time (HT), which was different for each genotype. **B** & **D**) Same genotypes but grown at RT without vernalization. Points are averages of eight plants and error bars are standard errors of the means. Means with different letters are significantly different in Tukey test for that time point ($P < 0.05$). Note that the upregulation of *CO1* after the return of the plants from vernalization occurred only in the *vrn1* mutant that has no functional copies of *VRN1*.

CO2 transcripts were downregulated during vernalization and showed a sharp increase when we moved the plants to RT. However, in contrast to *CO1*, this increase was observed in all three genotypes (Fig 6C-D). After this increase, *CO2* transcript levels remained high in the flag leaves during heading and showed no significant differences between the *vrn1* and the spring *vrn-B1*

460 mutant (Fig 6C-D). These results indicate that *VRN1* has a smaller effect on the regulation of
461 *CO2* than on the regulation of *CO1*.

462

463 **Effect of photoperiod and phytochromes on the transcriptional regulation of *CO1* and *CO2***

464 The strong upregulation of *CO1* in the *ppd1* mutant indicated that *PPD1* is a transcriptional
465 repressor of *CO1* (Fig 4A). Since phytochromes *PHYC* [15] and *PHYB* [31] are both required for
466 the LD transcriptional activation of *PPD1*, we explored the effect of mutations in these two
467 phytochromes on the expression profiles of *CO1* and *CO2*. To do this, we used recently
468 published RNAseq studies for leaf samples (4th leaf, ZT 4h) from loss-of-function mutants *phyB*
469 and *phyC* in Kronos-PI under both LD [31] and SD conditions [32].

470 A factorial ANOVA for transcripts per million reads (TPM) using photoperiod (LD and SD) and
471 genotype (WT, *phyC* and *phyB*) as factors, revealed significant differences between SD and LD
472 for all four genes (*CO-A1*, *CO-B1*, *CO-A2* and *CO-B2*, S4 Fig). We also detected difference
473 between genotypes and genotype x photoperiod interactions for the *CO1* homeologs but not for
474 the *CO2* homeologs. The significant interaction was associated with the LD downregulation of
475 *CO1* homeologs in the wild type and their upregulation in the *phyB* and *phyC* mutants (S4 Fig).
476 Both *CO2* homeologs were upregulated by LD and showed no significant differences between
477 wild type and *phy* mutants. *CO-B2* showed significantly higher transcript levels than *CO-A2* for
478 all genotypes (S4 Fig), whereas for *CO1* the transcript levels and the differences were larger in
479 *CO-A1* relative to *CO-B1*.

480

481

482 **Protein-protein interactions among CO1, CO2, PPD1, VRN2, PHYC and PHYB**

483 To test if the interactions among *CO1*, *CO2* and *PPD1* observed at the genetic and
484 transcriptional levels were associated with interactions at the protein level, we performed yeast-
485 two-hybrid (Y2H) and split yellow fluorescent protein (YFP) assays among the three proteins. In
486 a previous study, we reported positive Y2H interactions between the CCT domains of CO1 and
487 CO2, but not between these two proteins and a truncated version of PPD1 including the CCT
488 domain [33]. In this study, we used a complete PPD1 protein and detected strong Y2H
489 interactions between PPD1 and both CO1 and CO2. The Y2H interaction between PPD1 and
490 CO1 was stronger than between PPD1 and CO2 (Fig 7A).

491 We further validated the interactions between CO1 and CO2 (Fig 7B) and between CO1 and
492 PPD1 (Fig 7C-D) using split-YFP assays in wheat protoplasts. We initially failed to detect the
493 split-YFP interaction between CO1 and PPD1 in Kronos, so we used protoplasts extracted from
494 an early flowering loss-of-function mutant for *elf3* in Kronos, which has increased levels of
495 *PPD1* transcripts [29, 34]. We were able to detect the CO1-CO2 and CO1-PPD1 interactions
496 (but not the CO2-PPD1) by split-YFP in the *elf3* mutant when protoplasts were exposed to light.
497 For both CO1 and PPD1, we detected the proteins by Western blots only after we exposed the
498 protoplasts to light but not when we incubated them in the dark after transfection, suggesting that
499 light is required to stabilize these proteins.

500

501

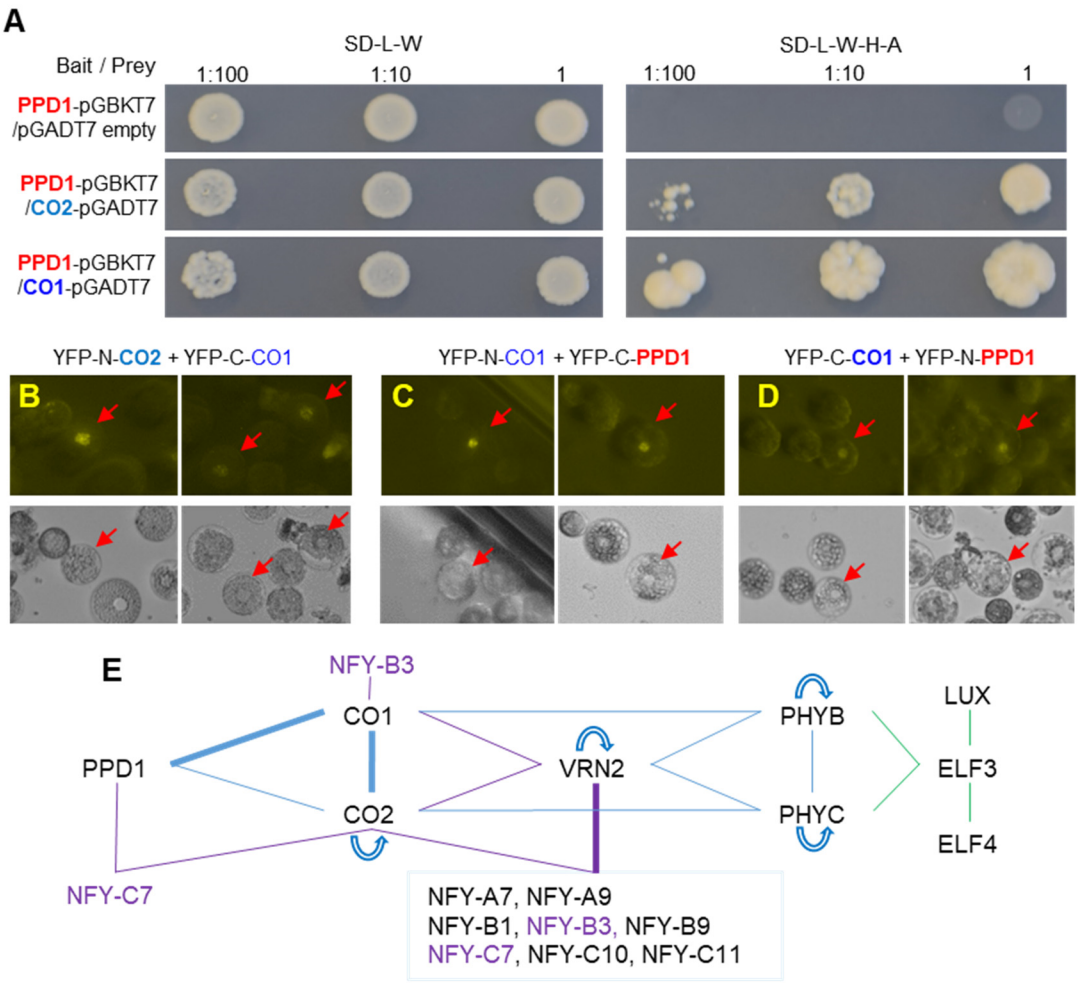

Fig 7. Protein interactions. (**A**) Yeast-two-hybrid (Y2H) interactions between PPD1 and CO1 or CO2. Left panel: SD medium lacking Leucine and Tryptophan (SD-L-W) to select for yeast transformants containing both bait and prey. Right panel: interaction on SD-L-W-H-A medium (no L, W, H and A). Dilution factors = 1, 1:10 and 1:100. (**B-D**) Split-YFP in wheat protoplast. (**B**) Positive nuclear interactions between CO1 and CO2. (**C-D**) Positive nuclear interactions between CO1 and PPD1 in two different YFP-N/YFP-C configurations. (**E**) Summary of Y2H interactions among wheat CO1, CO2, PPD1, VRN2, PHYB, PHYC, and ELF3 from S5 Fig. Green lines are based on published results from *Brachypodium* [35] and violet lines on published results from wheat [24]. Thick lines indicate interactions validated by split-YFP in wheat protoplasts (blue) or *in vitro* coIP (violet). Curved arrows indicate self-dimerization**.**

514 Finally, we tested pairwise interactions among CO1, CO2, PPD1, VRN2, PHYC and PHYB
515 proteins by Y2H assays (Figs 7E and S5 Fig). In addition to interacting with CCT-domain
516 proteins PPD1 (Fig 7A) and VRN2 [33], CO1 and CO2 showed positive interactions with both
517 PHYC and PHYB (Fig 7E and S5 Fig) in the Y2H assays. The interaction between CO1 and
518 PHYC was stronger than between CO1 and PHYB, whereas the interaction between CO2 and
519 PHYB was stronger than between CO2 and PHYC. Both phytochromes showed positive
520 interactions with VRN2 but not with PPD1 (Fig 7E and S5 Fig). In addition, we showed that the
521 full length PPD1 protein did not interact with VRN2 in Y2H (S5 Fig). CO2, VRN2, PHYC and
522 PHYB were able to form homodimers [15, 33] but not CO1 or PPD1 (S5 Fig). The diagrammatic
523 representation of these interactions reveals an extensive and complex network of protein-protein
524 interactions, with CO1 and CO2 providing a connection between the LD flowering promoter
525 PPD1 and the LD flowering repressor VRN2 (Fig 7E).

526

527 **Discussion**

528 **Genetic interactions among *CO1*, *CO2, PPD1* and *VRN2* modulate photoperiodic responses**
529 **in grasses**

530 ***Long day grasses***

531 Natural variation in wheat heading time in response to photoperiod has been mapped mainly to
532 the three *PPD1* homeologs [16, 17, 36]. Similarly, a genome wide association study of 220
533 spring barley varieties found that most of the variation in heading time (31%) was associated
534 with the *PPD1* locus and variation in the *CO1* locus had a limited contribution (<5%) [37].
535 These results agree with the limited effect on heading time detected in this study in the Kronos

536 *co1*, *co2*, and *co1 co2* mutants compared with the large differences detected between *PPD1*
537 alleles (Fig 2) and mutants (Fig 4). Even when both *CO1* and *CO2* homeologs were replaced
538 with truncated mutants (*co1 co2*), plants headed only three days earlier than the wild type under
539 LD and 13 days earlier under SD (Fig 2). By contrast, loss of function mutations in *PPD1*
540 delayed heading time approximately two months in LD (Fig 4), and differences between the
541 *Ppd-A1a* and *Ppd-A1b* alleles were even larger under SD (Fig 2).

542 The effect of the *co1 co2* mutations on the acceleration of heading time was small, but highly
543 significant ($P < 0.0001$) and consistent across experiments under LD in Kronos-PI and Kronos-
544 PS and under SD in Kronos-PI (Fig 2). This was an unexpected result because transgenic barley
545 plants overexpressing *CO1* [10] or *CO2* [11] flowered earlier than the wild type under both LD
546 and SD. These transgenic results had led to the general assumption that *CO1* and *CO2* operate as
547 flowering promoters in the temperate grasses. However, our results show that when *CO1* and
548 *CO2* are expressed under their native promoters in their expected tissues and developmental
549 stages (and in the presence of functional *PPD1* and *VRN2* alleles) they operate mainly as mild
550 LD and SD flowering repressors rather than as flowering promoters (except for *CO2* in Kronos-
551 PS under LD, Fig 2).

552 This inconsistency may be generated by the elevated and ectopic expression levels of *Ubi::CO1*
553 and *Ubi::CO2* in the transgenic plants, but also by differences in the genetic backgrounds. The
554 two transgenic barley lines were developed in the variety Golden Promise [10], which carries the
555 *ppd-H1* allele with reduced sensitivity to LD and does not have any functional copy of *VRN2*. By
556 contrast, Kronos has functional *PPD1* and *VRN2* genes. Our results show that in a Kronos line
557 with no functional copies of *PPD1* (*ppd1*), *CO1* accelerates heading time under LD (Fig 4)
558 similarly to the overexpression of *CO1* in Golden Promise. In addition, the downregulation of

559 *VRN2* in the Kronos *co1 co2* mutant may have contributed to the earlier heading time of these
560 mutants (Fig 2), whereas no interactions with *VRN2* are possible in Golden Promise.

561 The previous results suggest the existence of complex genetic interactions among the
562 photoperiodic genes, a hypothesis that is also supported by significant digenic interactions in the
563 factorial ANOVA including *CO1*, *CO2* and *PPD1* (Table S3). The three-way interaction among
564 the three genes was also significant, which reflects the differences in digenic interactions
565 between *CO1* and *CO2* in Kronos-PS (significant) and Kronos-PI (not significant, Table S3).
566 The contribution of the *PPD1* x *CO2* interaction to the total sum of squares (9%) was more than
567 two-fold higher than the main *CO2* effect (4%), which suggests that a large part of *CO2* effect on
568 heading time was mediated by its modulation of the *PPD1* function (Table S3). Strong genetic
569 interactions between *CO1* and *PPD1* on heading time have also been reported in a barley
570 biparental population segregating for *Ubi::CO1* and the *ppd-H1* mutation [10] and in two
571 genome wide association studies (GWAS) in spring barley [37, 38]. In both GWAS, significant
572 effects of *CO1* on heading time were detected among the lines carrying the *ppd-H1* allele but not
573 among the lines carrying the functional wild type *Ppd-H1* allele [37, 38]. These strong genetic
574 interactions indicate that the effect of a particular photoperiod gene depends strongly on genetic
575 background, a result that has also been reported in the SD grasses as described in the next
576 section.

577 Although the effect of *CO1* on heading time is limited in the presence of functional *PPD1*
578 alleles, in the *ppd1* mutant background the presence of *CO1* was required for heading under LD
579 (Fig 4). It has been previously shown that hexaploid wheat plants with no functional *PPD1* genes
580 (but with wild type *CO1* alleles) were able to head under LD, and that these plants express *FT1*
581 although at lower levels [24]. These levels should be sufficient to send enough florigen to the

582 SAM to up-regulate both *VRN1* and GA biosynthesis and the subsequent induction of *LFY* and
583 *SOC1*, which are critical for timely spike development and stem elongation [18]. We hypothesize
584 that the inability of the spikes to emerge in the *ppd1 co1* mutants grown under LD or in the
585 Kronos-PS or *ppd1* mutants grown under SD, is associated with insufficient production of *FT1* in
586 the leaves, which results in limited levels of GA, *LFY* and *SOC1* in the SAM. Addition of
587 exogenous GA to photoperiod sensitive *T. monococcum* genotypes that express *VRN1* under SD
588 (due to a deletion in the *VRN1* promoter) has previously been shown to partially rescue the arrest
589 in spike development and stem elongation under SD [18].

590

591 ***Short day grasses***

592 In most sorghum genotypes, *SbCO1* operates as a flowering promoter in SD and as a flowering
593 repressor in LD [39] and *SbPRR37* as a flowering repressor in LD [14, 40]. By contrast, the
594 orthologous *PPD1* gene in barley and wheat functions as a LD heading promoter [12, 16, 19]
595 (Fig 4). In spite of the opposite roles, the genetic interactions between *PRR37/PPD1* and *CO1*
596 showed some similarities. In a sorghum population segregating for *SbCO1* and *SbPRR37*, *SbCO1*
597 showed a large effect on heading time among the plants carrying the non-functional *Sbprr37*
598 allele (48% of the variation), but had no effect among the plants carrying the functional *SbPrr37*
599 allele [41]. This is similar to the GWAS results in spring barley described above [37, 38] and
600 consistent with the stronger effect of the *co1* mutation in the *ppd1* mutant than in the sister lines
601 carrying functional *PPD1* alleles described in this study.

602 Similar to sorghum, in most rice genotypes, *OsPRR37* (=*Hd2*) works as a LD flowering
603 repressor [13] and *OsCO1* (=*Hd1*) as both a LD flowering repressor and a SD flowering
604 promoter. Interestingly, transformation of a rice line deficient in *OsCO1* function with a wheat

605 *CO2* genomic clone accelerated flowering in SD and delayed flowering in LD, complementing
606 the *OsCO1* function [42]. Since our results indicate that wheat *CO2* functions as a SD flowering
607 repressor (Fig 2A), the rice result suggests that the function of the wheat CO2 protein was altered
608 when it was expressed in rice. The opposite change was observed when a late-flowering
609 Arabidopsis *prr7* mutant was transformed with rice *OsPRR37* driven by the Arabidopsis *PRR7*
610 promoter. When expressed in Arabidopsis, *OsPRR37* functioned as a LD promoter of flowering
611 in spite of its normal role as a LD repressor of flowering in rice. Based on these results, it is
612 tempting to speculate that the different roles of *PRR37/PPD1* and *CO2* in SD and LD grasses
613 may be the result of differences in the balance of multiple epistatic interactions among the genes
614 involved in the photoperiodic response, rather than a difference in the specific function of their
615 encoded proteins.

616 This hypothesis is also supported by changes in gene function reported in sorghum and rice
617 plants carrying loss-of-function mutations in both *PRR37* (*prr37*) and *GRAIN NUMBER, PLANT*
618 *HEIGHT, AND HEADING DATE7* (*ghd7,* a *VRN2* ortholog [43]). In the *prr37 ghd7* sorghum
619 and rice mutants, *CO1* function changed from a flowering repressor to a flowering promoter in
620 LD, while maintaining its usual role as a flowering promoter in SD [41, 44, 45]. In addition, in
621 most rice genotypes carrying the *ghd7* mutation *OsPRR37* function changes from a SD promoter
622 to a SD repressor of heading, while maintaining its role as a LD flowering repressor [46].
623 Genetic interactions between *VRN2* (*GHD7*) and both *CO1* (*Hd1*) [47] and *CO2* [11] have been
624 reported also in barley, suggesting that similar mechanisms may exist in the temperate cereals.
625 Taken together, these results indicate that genetic interactions between *PPD1/PRR37*,
626 *VRN2/GHD7* and *CO1/CO2* play a central role in the regulation of heading time in response to

627 photoperiod in both LD- and SD-grasses and that, therefore, the effect of particular genes may
628 vary in different genetic backgrounds.

629

630 **Complex interactions at the transcriptional level contribute to the observed genetic**
631 **interactions on heading time**

632 The significant upregulation of *CO1* in the *ppd1* mutant under LD (Fig 5A and S3A Fig)
633 suggests that *PPD1* may function as a transcriptional repressor of *CO1* under this condition. This
634 hypothesis is supported by the upregulation of *CO1* in the *phyB* and *phyC* mutants (S4 Fig),
635 where *PPD1* transcription is strongly downregulated [15, 31], and by the negative correlation
636 between *PPD1* and *CO1* transcript levels in both *ppd1* triple mutants of hexaploid wheat
637 'Paragon' under LD [24], and photoperiod sensitive and insensitive isogenic lines of Paragon
638 under SD [48]. Under SD, however, the *CO1* transcription peak in the *ppd1* mutant was slightly
639 lower than the peaks of the genotypes with functional *PPD1* alleles, which showed an 8 h shift
640 (Fig 5A). These results indicate that *PPD1* has an effect on *CO1* expression under SD, but not as
641 a transcriptional repressor as in LD (Fig. 5A). Under SD, both *CO1* and *PPD1* have a
642 transcription peak at ZT8 (Fig 5A and 5C).

643 Since *PPD1* induces the expression of *VRN1* under LD, and *VRN1* represses *CO1* transcription
644 (Fig 6), we cannot rule out the possibility that the effect of *PPD1* on *CO1* transcription is
645 mediated, at least in part, by *VRN1*. When Kronos *vrn-A1*, *vrn-B1* and *vrn1* mutants were
646 returned to room temperature after vernalization, *CO1* was rapidly upregulated in the leaves of
647 the *vrn1* mutant but not in the other three genotypes with functional *VRN1* copies (Fig 6). An
648 identical expression profile has been described before for *VRN2* in the same mutants [23],
649 indicating that *VRN1* functions as a LD transcriptional repressor of both *CO1* and *VRN2*.

650 *CO2* transcript levels were not significantly affected by the different *PPD1* alleles under LD or
651 SD (Fig 5B) or by the loss-of-function mutants of *VRN1* in a LD experiment (Fig 6C-D).
652 Similarly, no changes in *CO2* transcription were observed between Paragon-PI and Paragon-PS
653 lines grown under SD [48], between Kronos-PI and the *phyB* or *phyC* mutants (S4 Fig), or
654 between Kronos-PS and *ppd1* mutants (S3B Fig). However, mutations in *co2* affected the LD
655 diurnal transcriptional profiles of all the flowering genes presented in Fig 5. Under LD, *CO1*
656 transcript levels were more than 2-fold higher in the *co2* mutant than in the Kronos-PS control at
657 the ZT12 peak (Fig 5A), suggesting that CO2 functions as a negative transcriptional regulator of
658 *CO1*. This is also supported by the downregulation of *CO1* transcripts in a barley line
659 overexpressing *CO2* [11]. The effect of *CO2* on *CO1* transcription may contribute to the
660 significant genetic interaction on heading time observed between *CO1* and *CO2* in this study
661 (Table S3b).

662 Overexpression of *CO1* and *CO2* in winter barley was associated with the upregulation of *VRN2*,
663 both under LD and SD, where *VRN2* is not normally expressed [11]. A similar upregulation of
664 *VRN2* has been reported in *Brachypodium* plants overexpressing *CO1* under LD [49]. By
665 contrast, knock-down of *CO1* expression in *Brachypodium* [49] or loss-of-function mutants in
666 *co1*, *co2*, or *co1 co2* in Kronos in our study (Fig 5F) were associated with the down regulation of
667 *VRN2* transcripts in LD (and SD in Kronos PI). The regulation of *VRN2* by CO1 may be direct,
668 as it was recently shown in rice that a complex formed by Hd1 (CO1), GHD8 and OsHAP5b can
669 bind the promoter of *GHD7* (*VRN2*) and activate its transcription [50]. Taken together, these
670 results are consistent with *CO1* and *CO2* being promoters of *VRN2* transcription in the temperate
671 grasses, a role that is likely more important during the fall than in the spring, when high
672 expression of *VRN1* results in the downregulation of both *CO1* and *VRN2*.

673 Photoperiod and vernalization genes converge on the regulation of *FT1*, whose transcript levels
674 are well correlated with heading time [11, 51]. Here we also observed a good correlation
675 between *FT1* transcript levels and heading time both under LD and SD (Fig 2 and 5D). Since
676 *PPD1* is a critical LD transcriptional promoter of *FT1* [12, 35], it was not surprising to see
677 almost undetectable levels of *FT1* in the *ppd1* mutant, which were correlated with low *VRN1*
678 transcript levels and late heading time under LD (Fig 5D-E). The low transcript levels of *VRN1*
679 in the *ppd1* mutant may have contributed to the slight increase in *VRN2* transcript levels
680 observed in this mutant (Fig 5F), because *VRN1* is a known transcriptional repressor of *VRN2* in
681 wheat under LD [23, 52].

682 The transcriptional profiles of *VRN1* under SD were unexpected. The increased levels of *FT1* in
683 the two Kronos-PI genotypes (Fig 5D), were not reflected in the upregulation of *VRN1* (Fig 5E).
684 This suggests that either some factors required for the *VRN1* up-regulation by *FT1* [53] are
685 missing, or the presence of one or more additional SD repressors. If has been previously shown
686 that deletions in a CArG box located in the *VRN1* promoter in photoperiod sensitive *T.*
687 *monococcum* are associated with increased *VRN1* transcript levels under SD, suggesting the
688 existence of a SD repression mechanism of *VRN1* transcription [20]. The upregulation of *VRN1*
689 in the *ppd1* mutant under SD (Fig 5E) suggests the possibility that *PPD1* may be involved in this
690 SD repression mechanism. A strong SD upregulation of *VRN1* has also been reported in *phyC*
691 and *phyB* mutants of Kronos-PI, which also showed a significant down-regulation of *PPD1* [32].
692 Under LD, the high transcript levels of *VRN2* in the *ppd1* mutant indicates that *PPD1* is not
693 required for the LD expression of *VRN2* (Fig 5F). Under SD, however, *VRN2* was expressed only
694 in Kronos-PI and Kronos-PI *co1 co2* (Fig 5F), which are the only genotypes that show a
695 significant increase in *PPD1* transcripts during the night (ZT16, Fig 5C). Since a short pulse of

696 light in the middle of the night induces *PPD1* transcription and is sufficient to greatly accelerate
697 Kronos-PS flowering in SD [19], we speculate that the higher transcript levels of *PPD1* during
698 the night in the two Kronos-PI lines (particularly at ZT16) may be important for the acceleration
699 of heading time under SD. The positive role of *PPD1* on the upregulation of *VRN2* under SD has
700 also been reported in hexaploid wheat lines carrying the photoperiod insensitive *Ppd-D1a* allele
701 but not in sister lines carrying the photoperiod sensitive *Ppd-D1b* allele [54], and in young winter
702 barley plants [11].

703 The role of *PPD1* on the upregulation of *VRN2* and *FT1* is also reflected in their similar
704 transcription profiles in Kronos-PS under LD (Fig 5C, D and F, blue lines). However, those
705 similarities disappear in the different *CO1* and *CO2* mutants, which suggests that the effect of
706 *PPD1* on *FT1* and *VRN2* under LD is modulated by *CO1* and *CO2*. Under SD, the altered
707 expression of *PPD-A1a* (promoter deletion) in Kronos-PI has two opposing effects, the up-
708 regulation of *FT1* that promotes flowering (Fig 5D) and the up-regulation of *VRN2* that represses
709 flowering (Fig 5F). This may contribute to the lower *FT1* transcript levels in Kronos-PI (higher
710 *VRN2*) relative to Kronos-PI *co1 co2* (lower *VRN2* levels) under SD (Fig 5D and F).

711 To summarize the dynamics of these transcriptional interactions during the seasons, we propose
712 the following working model for the ancestral photoperiod sensitive winter wheats. In the fall,
713 *PPD1*, *CO1* and *CO2* promote the expression of *VRN2* in the leaves, which prevents flowering
714 by repressing the transcriptional induction of *FT1*. During the winter, the increase in *VRN1*
715 expression in the apex [22] promotes the initial stage of reproductive development whereas its
716 upregulation in the leaves results in the gradual downregulation of both *VRN2* and *CO1*, which
717 facilitates the promotion of *FT1* by *PPD1* and the acceleration of spike development and stem
718 elongation in the spring.

719

720 **Protein-protein interactions add an additional level of regulation to wheat heading time**

721 In addition to the complex transcriptional interactions described above, the proteins encoded by
722 the photoperiod genes form an intricate network of protein-protein interactions that contribute an
723 additional layer of complexity to the photoperiodic regulation of heading time. In Arabidopsis,
724 the central photoperiod gene *CO* is regulated at the transcriptional and posttranscriptional level.
725 A complex transcriptional regulation is required to establish the presence of *CO* mRNA during
726 the evening of a long day, when light can stabilize the CO protein, resulting in the activation of
727 *FT* transcription [27].

728 Several PRR proteins promote flowering in Arabidopsis by interacting with and stabilizing the
729 CO protein during the day specifically under LD, and indirectly through their roles in the
730 circadian clock [55]. Mutations in *PRR* genes delay Arabidopsis flowering under LD but not
731 under SD (similar to *PPD1* in wheat), with double mutants showing a stronger delay [56]. The
732 late-flowering Arabidopsis *prr7* mutant can be complemented by rice *OsPRR37* [57], suggesting
733 some conserved functions in rice and Arabidopsis. In this study, we detected interactions
734 between wheat PPD1 full-length protein and both CO1 and CO2 in Y2H and validated the CO1-
735 PPD1 interactions by split-YFP (Fig 7). These results suggest that the interactions between CO
736 and PRRs likely precede the split between monocot and dicot plants.

737 In spite of these similarities, there are also important differences between the grass *PPD1/PRR37*
738 gene and the homologous *PRR* genes from Arabidopsis. The Arabidopsis *PRR* genes are part of
739 the circadian clock and their mutants affect the expression of circadian clock genes and their
740 multiple downstream targets. By contrast, the natural mutation in the barley photoperiod
741 insensitive *ppd-H1* allele did not affect diurnal or circadian cycling of barley clock genes [58].

742 This result suggests that after the duplication that generated *PRR37* and *PRR73* in the grasses,
743 which is independent of the Arabidopsis duplication that originated *PRR3* and *PRR7*,
744 *PRR37/PPD1* acquired a more specialized role in the photoperiodic response with a more limited
745 role in the circadian clock.

746 In addition to its interactions with the LD flowering promoter PPD1, CO1 and CO2 can form
747 heterodimers with the LD flowering repressor VRN2, which is also a member of the CCT
748 domain protein family [33]. We hypothesize that the interactions with VRN2 might be relevant
749 to *CO1* and *CO2* function because loss-of-function mutation in *ghd7/vrn2* result in reversals of
750 functional in *OsPRR37* (*Hd2*) [46] and *OsCO1* (*Hd1*) in rice [44, 45], and *SbCO1* in sorghum
751 [41]. In rice, GHD7 binds to the transcription-activating domain of OsCO1, probably weakening
752 or blocking the transcriptional activation of *Ehd1* and *Hd3a* [45]. We have initiated crosses
753 among Kronos lines with mutations in *vrn2* [30], *co1*, *co2*, and *ppd1* to test these interactions in
754 wheat.

755 Recent studies in rice showed that another CCT-domain protein, the NUCLEAR
756 TRANSCRIPTION FACTOR Y subunit B-11 (NF-YB11 = HEME ACTIVATOR PROTEIN or
757 HAP-3H = *Ghd8*) has large effects on heading time and significant genetic interactions with
758 *OsGHD7*, *OsCO1* and *OsPRR37* [46]. We have previously shown that in addition to interacting
759 with each other, CO2 and VRN2 interact with the same subset of eight NUCLEAR FACTOR-Y
760 (NF-Y) transcription factors (Fig 7E) [33], suggesting an additional functional connection
761 between these proteins. This connection through the NF-Y proteins seems to less extensive
762 between CO1 and VRN2, where only one shared NF-Y interactor has been identified so far (Fig
763 7E) [33]. Members of the NF-Y family have been shown to be involved in the regulation of
764 flowering through interactions with CCT domain proteins CO and COL in other plant species

765 [59-61]. Using yeast-three-hybrid (Y3H) assays, we previously showed that VRN2 competes
766 with CO2 for interactions with the NF-Ys, and that mutations in three conserved arginine (R)
767 residues within the CCT domain of VRN2 reduce the strength of the protein interactions and
768 competition with CO2 [33]. Since these same mutations abolish or reduce VRN2 function as a
769 LD flowering repressor, we hypothesize that the protein-protein interactions involving VRN2-
770 CO2-NF-Y CCT domain could be relevant for their function [33].

771 Phytochromes PHYB and PHYC are involved in the transcriptional regulation by light of both
772 *PPD1/PRR37* and *VRN2* in wheat [15, 31], *Brachypodium* [62], rice [63] and sorghum [40]. In
773 addition, OsPHYA, OsPHYB and OsGI proteins have been shown to interact directly with
774 OsGHD7, regulating protein stability [64]. We observed similar interactions between VRN2 and
775 both PHYB and PHYC in wheat. These two phytochromes also showed Y2H interactions with
776 CO1 and CO2, but not PPD1 (Fig 7E and S5). Additional experiments will be required to test if
777 these phytochrome interactions can stabilize the VRN2, CO1 and CO2 proteins in wheat as they
778 stabilize GHD7 in rice [64] or CO in Arabidopsis [65].

779 In summary, we found that CO1 and CO2 proteins can physically interact with each other and
780 with both PPD1 (a central LD flowering promoter) and VRN2 (a central LD flowering
781 repressor), providing a physical link between these central photoperiodic proteins (Fig 7E).
782 Among the 15 pairwise interactions tested among PHYB, PHYC, PPD1, CO1, CO2 and VRN2
783 80% showed positive interactions in Y2H assays indicating a complex and dense network of
784 protein interactions. We hypothesize that this network of protein interactions provides an
785 additional layer of molecular mechanisms that result in the complex genetic interactions in
786 heading time detected in this study.

787

788 **Two interacting photoperiod pathways in grasses**

789 A central conclusion of our study is that *PPD1* can perceive the differences in photoperiod and
790 adjust heading time accordingly even in the absence of any functional copy of *CO1* or *CO2.*
791 Similarly, *CO1* can accelerate heading time under LD in the absence of a functional copy of
792 *PPD1*. This is also true in rice, where heading time differences between SD and LD are observed
793 for *OsCO1* alleles in *Osprr37* mutants, and for *OsPRR37* alleles in rice *Osco1* mutants [46].
794 These results suggest that grasses have either two photoperiod pathways, each of them capable of
795 perceiving the length of the day/night and of regulating heading time, or a single point of
796 perception of the differences in photoperiod upstream of *PPD1* and *CO1*, which can then
797 transmit the signal to both genes. Recently, it has been suggested that the dark reversion of the
798 Pfr form of PHYC may be involved in measuring night length (molecular hourglass model), by
799 modulating the accumulation of the ELF3 protein, a direct transcriptional repressor of *PPD1*
800 [35]. This mechanism is different from the external coincidence model proposed for Arabidopsis
801 [66]. Although we favour the hypothesis of separate mechanisms for *PPD1* and *CO1* perception
802 of photoperiod, we currently cannot rule out the possibility that, in the temperate grasses, ELF3
803 mediates both the *PPD1* and *CO1* responses to photoperiod.

804 Another important conclusion from our study and from previous studies in sorghum and rice [40,
805 44, 46], is that the *CO* and *PRR37/PPD1* photoperiod pathways are extensively interconnected.
806 Changes in the balance of these interactions seem to play a central role in the diversity of
807 photoperiod responses in grasses, as suggested by changes in function observed when
808 photoperiodic genes are swapped between LD and SD species or when the same genes are
809 expressed in different mutant backgrounds in its own species. The different expression profiles
810 of the photoperiodic genes in LD and SD also show that these interactions are dynamic and

811 affected by photoperiod. We hypothesize that the complex feedback transcriptional regulatory
812 loops and transcriptional interactions among photoperiod genes along with the intricate
813 interactions among their encoded proteins contribute to the complex genetic interactions in
814 heading time observed in this study and to the diversity of photoperiodic responses in grasses.

815

816 **Materials and methods**

817 **Plant materials**

818 The materials used in this study included the tetraploid wheat variety Kronos (*Triticum*
819 *turgidum* ssp. *durum*), which carries a functional and dominant *Vrn-A1* allele for spring growth
820 habit, a functional but recessive *vrn-B1* allele for winter growth habit, a functional *Vrn-B2* long
821 day repressor (*ZCCT-B2a* and *ZCCT-B2b* [30]), and the *Ppd-A1a* (photoperiod insensitive or PI)
822 allele that confers earlier flowering under short days resulting in a reduced photoperiodic
823 response. We also used in our study near-isogenic lines of Kronos carrying either the
824 photoperiod sensitive *Ppd-A1b* (PS) allele [18] or no functional alleles in the *PPD-A1* and *PPD-*
825 *B1* homeologs (*ppd1*) [19].

826 Using previously published wheat sequences for *CO1* [48] and *CO2* [42], and the Kronos
827 transcriptome [67] we identified the A and B coding sequences for *CO1* and *CO2* in Kronos and
828 deposited them in GenBank under accession numbers MT043302 (*CO-A1*), MT043303 (*CO-B1*),
829 MT043304 (*CO-A2*), MT043305 (*CO-B2*). We used those sequences to identify loss-of-function
830 mutations in *CO1* and *CO2* in the Kronos TILLING population [25, 26], which are described in
831 detail in the Results section. We then combined mutations in the A and B homeologs from each
832 gene to generate loss-of-function *co1* (henceforth *co1*) and *co2* mutants (henceforth *co2*). We
833 backcrossed the individual mutant lines with wild-type Kronos at least two times to reduce

834 background mutations and then combined all four homozygous mutations to produce a *co1 co2*
835 mutant (henceforth *co1 co2*). In addition to the wild type Kronos-PI, the four homozygous *Co1*
836 *Co2*, *co1 Co2*, *Co1 co2* and *co1 co2* allelic classes were generated in Kronos-PS and the *ppd1*
837 mutant. We were not able to recover the triple loss-of-function mutant *ppd1 co1 co2* from any of
838 the tested progenies.

839 **Phenotyping**

840 We stratified wheat grains at 4 °C for 2 d in the dark and after germination we planted them in
841 pots in the soil. We evaluated the mutant and control lines in CONVIRON growth chambers with
842 metal halide bulbs supplemented by florescent bulbs set to 22 °C during daylight and 17 °C
843 during dark periods. Lights were set to 260-300 μmol m^{-2} s^{-1} and were on for 16 h in LD
844 experiments and 8 h in short day (SD) experiments. We recorded heading time as the total time
845 from planting in soil to full emergence of the spike from the sheath. Spikes were threshed and
846 total grain number counted per spike.

847 **Statistical analysis**

848 We compared heading time in different genotypes using one-way ANOVAs for single locus and
849 factorial ANOVAs for two or more loci. We tested homogeneity of variances using the Levene's
850 test and normality of residuals with the Shapiro–Wilks test. We transformed the data when
851 necessary to satisfy the ANOVA assumptions. We performed all statistical analyses using SAS
852 9.4 (SAS Institute). Error bars in all graphs are standard errors of the means (s.e.m.).

853 **Gene expression analysis**

854 To study the effect of *ppd1*, *co1* and *co2* mutant alleles on the transcription profiles of genes
855 affecting wheat flowering, we collected leaves from plants grown in a growth chamber under LD

856 using the same settings as described in the previous phenotypic section. For the time course
857 experiment, we collected samples in liquid nitrogen every 4 h throughout the day from the newly
858 expanded fourth leaf. In this experiment, we included the *ppd1* mutant and all four possible
859 combinations of the *CO1* and *CO2* wild type and mutant alleles in the Kronos-PS (*Ppd-A1b*)
860 background.

861 RNA was isolated from leaves using the Spectrum Plant Total RNA Kit (Sigma-Aldrich)
862 following the manufacturer's recommendations. We treated the RNA samples with DNase
863 (Promega) according to the manufacturer's protocol prior to first-strand cDNA synthesis. We
864 assessed RNA integrity by a combination of A260/A280 and A260/A230 measurements and
865 running samples on a denaturing formaldehyde-agarose gel as recommended in the Qiagen
866 RNAeasy Mini Handbook. We used only samples with 260/280 and 260/230 ratios > 1.7 and no
867 degradation. We synthesized cDNA using 2.0 µg of total RNA per sample and M-MLV Reverse
868 Transcriptase (Promega) and poly-T primers (Sigma-Aldrich).

869 We performed the quantitative reverse transcription-PCR (qRT-PCR) assays using SybrGreen
870 Takara Master Mix in a 7500 Fast Real-Time PCR system (Applied Biosystems). For PCR, we
871 used one cycle at 95°C for 30 s and 40 cycles of 95°C for 5 s, 60°C for 5 s, and 72°C for 34 s,
872 followed by a melting curve program. We quantified expression using the delta Ct method (2^{-}
873 $^{\Delta CT}$) with *ACTIN* as endogenous control [15]. Primer efficiencies were all > 95% and their
874 sequences are summarized in Table S5. Primer sequences were previously described for *FT1* and
875 *VRN1* [51], *PPD1* [48], *CO1* and *CO2* [15] and *VRN2* [30].

876 **Yeast-two-hybrid (Y2H) and split yellow fluorescent protein (YFP) assays**

877 The full-length coding region of PPD1 was amplified from Kronos and the PHYB truncations
878 were amplified from *Triticum monococcum* with primers listed in Supplementary Table S5. The
879 amplified fragments were cloned into yeast vectors pGBKT7 and pGADT7 (Clontech,
880 http://www.clontech.com/), which were used to transform yeast strain Y2HGold (Clontech)
881 using the lithium acetate method. Transformants were selected on SD medium lacking leucine
882 (L) and tryptophan (W) plates and re-plated on SD medium lacking L, W, histidine (H) and
883 adenine (A) to test the interactions. Yeast vectors for VRN2 (full-length, both bait and prey),
884 CO1 (prey, including both B-boxes and CCT domain, amino acids 10 to 379) and CO2 (prey,
885 including both B-boxes and CCT domain, 15 to 356 amino acids) were previously described in
886 [33], and those for PHYC (N-PHYC, C-PHYC and FL-PHYC) and full-length PHYB (as prey)
887 in [15]. CO1 and CO2 showed strong auto-activation when used as baits so they were only used
888 as preys. The full-length PHYB gave strong autoactivation when used as bait, so we generated
889 two additional truncations N-PHYB and C-PHYB (primers in Table S5). Only N-PHYB can be
890 used as bait without autoactivation, and all three (N-PHYB, C-PHYB and FL-PHYB) can be
891 used as preys in Y2H assays. The truncated versions of PHYC include amino acids 1–600 (N-
892 terminal) and 601-1139 (C-terminal) [15], and those for PHYB amino acids (1-625 (N-terminal)
893 and 626-1166 (C-terminal).

894 For the bi-molecular fluorescent complementation (BiFC or split YFP) assays, each set of wheat
895 proteins was recombined into modified Gateway-compatible pY736 and pY735 which contain
896 the *UBIQUITIN* promoter to generate YFP-N-terminal fragment and YFP-C-terminal-fragment
897 fusion proteins. Wheat protoplasts were prepared, transfected and visualized as described in [68]

898

899 **ACKNOWLEDEMENTS**

900 This project was supported by NRI Competitive Grants 2017-67007-25939 and 2016-67013-
901 24617 from the USDA National Institute of Food and Agriculture (NIFA) and by the Howard
902 Hughes Medical Institute. Daniel Woods is a Howard Hughes Medical Institute Fellow of the
903 Life Sciences Research Foundation.

904

905 **AUTHOR CONTRIBUTIONS**

906 Lindsay M. Shaw: Investigation, Writing - Original Draft -Review & Editing. Chengxia Li:
907 Investigation, Writing - Original Draft -Review & Editing. Daniel Woods: Investigation, Writing
908 -Review & Editing. Maria A. Alvarez: Investigation, Writing -Review & Editing. Huiqiong:
909 Investigation, Methodology, Writing -Review & Editing. Mei Yee Lau: Investigation. Andrew
910 Chen: Investigation, Writing -Review & Editing. Jorge Dubcovsky: Conceptualization, Formal
911 analysis, Supervision, Project administration and funding acquisition, Writing –extensive Review
912 & Editing.

913

914 **CONFLICT OF INTEREST**

915 The authors declare that they do not have any conflict of interest.

916

917 **REFERENCES**

918 1. Bouche F, Woods DP, Amasino RM. Winter memory throughout the plant kingdom:
919 different paths to flowering. Plant Physiol. 2017;173(1):27-35. doi: 10.1104/pp.16.01322.
920 PMID: 27756819.

921 2. Garner WW, Allard HA. Effect of the relative length of day and night and other factors of
922 the environment on growth and reproduction in plants. J Agric Res. 1919;18:0553-606.
923 PMID: WOS:000188347200038.
924 3. Andres F, Coupland G. The genetic basis of flowering responses to seasonal cues. Nat
925 Rev Genet. 2012;13(9):627-39. doi: 10.1038/nrg3291. PMID: 22898651.
926 4. Suarez-Lopez P, Wheatley K, Robson F, Onouchi H, Valverde F, Coupland G.
927 CONSTANS mediates between the circadian clock and the control of flowering in
928 Arabidopsis. Nature. 2001;410(6832):1116-20. doi: 10.1038/35074138. PMID:
929 11323677.
930 5. Yanovsky MJ, Kay SA. Molecular basis of seasonal time measurement in Arabidopsis.
931 Nature. 2002;419(6904):308-12. doi: 10.1038/nature00996. PMID: 12239570.
932 6. Putterill J, Robson F, Lee K, Simon R, Coupland G. The CONSTANS gene of
933 Arabidopsis promotes flowering and encodes a protein showing similarities to zinc finger
934 transcription factors. Cell. 1995;80(6):847-57. doi: 10.1016/0092-8674(95)90288-0.
935 PMID: 7697715.
936 7. Griffiths S, Dunford RP, Coupland G, Laurie DA. The evolution of *CONSTANS*-like
937 gene families in barley, rice, and Arabidopsis. Plant Physiol. 2003;131(4):1855-67. doi:
938 10.1104/pp.102.016188. PMID: 12692345.
939 8. Yano M, Katayose Y, Ashikari M, Yamanouchi U, Monna L, Fuse T, et al. Hd1, a major
940 photoperiod sensitivity quantitative trait locus in rice, is closely related to the Arabidopsis
941 flowering time gene CONSTANS. Plant Cell. 2000;12(12):2473-84. doi:
942 10.1105/tpc.12.12.2473. PMID: 11148291.

943 9. Higgins JA, Bailey PC, Laurie DA. Comparative genomics of flowering time pathways
944 using *Brachypodium distachyon* as a model for the temperate grasses. PLoS One.
945 2010;5(4):e10065. doi: 10.1371/journal.pone.0010065. PMID: 20419097.
946 10. Campoli C, Drosse B, Searle I, Coupland G, von Korff M. Functional characterisation of
947 *HvCO1*, the barley (*Hordeum vulgare*) flowering time ortholog of *CONSTANS*. Plant J.
948 2012;69(5):868-80. doi: 10.1111/j.1365-313X.2011.04839.x. PMID: 22040323.
949 11. Mulki MA, von Korff M. CONSTANS controls floral repression by up-regulating
950 *VERNALIZATION2* (*VRN-H2*) in Barley. Plant Physiol. 2016;170(1):325-37. doi:
951 10.1104/pp.15.01350. PMID: 26556793.
952 12. Turner A, Beales J, Faure S, Dunford RP, Laurie DA. The pseudo-response regulator
953 *Ppd-H1* provides adaptation to photoperiod in barley. Science. 2005;310(5750):1031-4.
954 doi: 10.1126/science.1117619. PMID: 16284181.
955 13. Koo BH, Yoo SC, Park JW, Kwon CT, Lee BD, An G, et al. Natural variation in
956 *OsPRR37* regulates heading date and contributes to rice cultivation at a wide range of
957 latitudes. Mol Plant. 2013;6(6):1877-88. doi: 10.1093/mp/sst088. PMID: 23713079.
958 14. Murphy RL, Klein RR, Morishige DT, Brady JA, Rooney WL, Miller FR, et al.
959 Coincident light and clock regulation of pseudoresponse regulator protein 37 (PRR37)
960 controls photoperiodic flowering in sorghum. Proc Natl Acad Sci U S A.
961 2011;108(39):16469-74. doi: 10.1073/pnas.1106212108. PMID: 21930910.
962 15. Chen A, Li C, Hu W, Lau MY, Lin H, Rockwell NC, et al. Phytochrome C plays a major
963 role in the acceleration of wheat flowering under long-day photoperiod. Proc Natl Acad
964 Sci U S A. 2014;111(28):10037-44. doi: 10.1073/pnas.1409795111. PMID: 24961368.

965 16. Beales J, Turner A, Griffiths S, Snape JW, Laurie DA. A pseudo-response regulator is
966 misexpressed in the photoperiod insensitive Ppd-D1a mutant of wheat (Triticum aestivum
967 L.). Theor Appl Genet. 2007;115(5):721-33. doi: 10.1007/s00122-007-0603-4. PMID:
968 17634915.
969 17. Wilhelm EP, Turner AS, Laurie DA. Photoperiod insensitive *Ppd-A1a* mutations in
970 tetraploid wheat (*Triticum durum* Desf.). Theor Appl Genet. 2009;118(2):285-94. doi:
971 10.1007/s00122-008-0898-9. PMID: 18839130.
972 18. Pearce S, Vanzetti LS, Dubcovsky J. Exogenous gibberellins induce wheat spike
973 development under short days only in the presence of *VERNALIZATION1*. Plant Physiol.
974 2013;163(3):1433-45. doi: 10.1104/pp.113.225854. PMID: 24085801.
975 19. Pearce S, Shaw LM, Lin H, Cotter JD, Li C, Dubcovsky J. Night-break experiments shed
976 light on the *Photoperiod1*-mediated flowering. Plant Physiol. 2017;174(2):1139-50. doi:
977 10.1104/pp.17.00361. PMID: 28408541.
978 20. Dubcovsky J, Loukoianov A, Fu D, Valarik M, Sanchez A, Yan L. Effect of photoperiod
979 on the regulation of wheat vernalization genes *VRN1* and *VRN2*. Plant Mol Biol.
980 2006;60:469-80.
981 21. Yan L, Loukoianov A, Blechl A, Tranquilli G, Ramakrishna W, SanMiguel P, et al. The
982 wheat *VRN2* gene is a flowering repressor down-regulated by vernalization. Science.
983 2004;303(5664):1640-4. doi: 10.1126/science.1094305. PMID: 15016992.
984 22. Yan L, Loukoianov A, Tranquilli G, Helguera M, Fahima T, Dubcovsky J. Positional
985 cloning of wheat vernalization gene *VRN1*. Proc Natl Acad Sci USA. 2003;100:6263-8.
986 23. Chen A, Dubcovsky J. Wheat TILLING mutants show that the vernalization gene *VRN1*
987 down-regulates the flowering repressor *VRN2* in leaves but is not essential for flowering.

988 PLoS Genet. 2012;8(12):e1003134. doi: 10.1371/journal.pgen.1003134. PMID:
989 23271982.
990 24. Shaw LM, Turner AS, Herry L, Griffiths S, Laurie DA. Mutant alleles of *Photoperiod-1*
991 in wheat (*Triticum aestivum* L.) that confer a late flowering phenotype in long days.
992 PLoS One. 2013;8(11):e79459. doi: 10.1371/journal.pone.0079459. PMID: 24244507.
993 25. Krasileva KV, Vasquez-Gross HA, Howell T, Bailey P, Paraiso F, Clissold L, et al.
994 Uncovering hidden variation in polyploid wheat. Proc Natl Acad Sci U S A.
995 2017;114(6):E913-E21. doi: 10.1073/pnas.1619268114. PMID: 28096351.
996 26. Uauy C, Paraiso F, Colasuonno P, Tran RK, Tsai H, Berardi S, et al. A modified
997 TILLING approach to detect induced mutations in tetraploid and hexaploid wheat. BMC
998 Plant Biol. 2009;9:115. doi: 10.1186/1471-2229-9-115. PMID: 19712486.
999 27. Valverde F. CONSTANS and the evolutionary origin of photoperiodic timing of
1000 flowering. J Exp Bot. 2011;62(8):2453-63. doi: 10.1093/jxb/erq449. PMID: 21239381.
1001 28. Waddington SR, Cartwright PM, Wall PC. A quantitative scale of spike initial and pistil
1002 development in barley and wheat. Ann Bot-London. 1983;51(1):119-30. PMID:
1003 WOS:A1983QC01200013.
1004 29. Alvarez MA, Tranquilli G, Lewis S, Kippes N, Dubcovsky J. Genetic and physical
1005 mapping of the earliness *per se* locus *Eps-A*^{m}*1* in *Triticum monococcum* identifies *EARLY*
1006 *FLOWERING 3* (*ELF3*) as a candidate gene. Funct Integr Genomic. 2016;16(4):365-82.
1007 doi: 10.1007/s10142-016-0490-3. PMID: 27085709.
1008 30. Distelfeld A, Tranquilli G, Li C, Yan L, Dubcovsky J. Genetic and molecular
1009 characterization of the *VRN2* loci in tetraploid wheat. Plant Physiol. 2009;149(1):245-57.
1010 doi: 10.1104/pp.108.129353. PMID: 19005084.

1011 31. Pearce S, Kippes N, Chen A, Debernardi JM, Dubcovsky J. RNA-seq studies using wheat
1012 *PHYTOCHROME B* and *PHYTOCHROME C* mutants reveal shared and specific
1013 functions in the regulation of flowering and shade-avoidance pathways. BMC Plant Biol.
1014 2016;16(1):141. doi: 10.1186/s12870-016-0831-3. PMID: 27329140.
1015 32. Kippes N, van Gessel C, Hamilton J, Akpinar A, Budak H, Dubcovsky J, et al. Effect of
1016 *phyB* and *phyC* loss-of-function mutations on wheat transcriptome under short and long
1017 day photoperiods. bioRxiv. 2020. doi: https://doi.org/10.1101/2020.04.07.030197.
1018 33. Li C, Distelfeld A, Comis A, Dubcovsky J. Wheat flowering repressor VRN2 and
1019 promoter CO2 compete for interactions with NUCLEAR FACTOR-Y complexes. Plant J.
1020 2011;67(5):763-73. doi: 10.1111/j.1365-313X.2011.04630.x. PMID: 21554456.
1021 34. Faure S, Turner AS, Gruszka D, Christodoulou V, Davis SJ, von Korff M, et al. Mutation
1022 at the circadian clock gene *EARLY MATURITY 8* adapts domesticated barley (*Hordeum*
1023 *vulgare*) to short growing seasons. Proc Natl Acad Sci U S A. 2012;109(21):8328-33.
1024 doi: 10.1073/pnas.1120496109. PMID: 22566625.
1025 35. Gao M, Geng F, Klose C, Staudt A-M, Huang H, Nguyen D, et al. Phytochromes
1026 measure photoperiod in *Brachypodium*. bioRxiv. 2019. doi: 10.1101/697169.
1027 36. Diaz A, Zikhali M, Turner AS, Isaac P, Laurie DA. Copy number variation affecting the
1028 *Photoperiod-B1* and *Vernalization-A1* genes is associated with altered flowering time in
1029 wheat (*Triticum aestivum*). PLoS One. 2012;7(3):e33234. doi:
1030 10.1371/journal.pone.0033234. PMID: 22457747.
1031 37. Stracke S, Haseneyer G, Veyrieras JB, Geiger HH, Sauer S, Graner A, et al. Association
1032 mapping reveals gene action and interactions in the determination of flowering time in

1033 barley. Theor Appl Genet. 2009;118(2):259-73. doi: 10.1007/s00122-008-0896-y. PMID:
1034 18830577.
1035 38. Alqudah AM, Sharma R, Pasam RK, Graner A, Kilian B, Schnurbusch T. Genetic
1036 dissection of photoperiod response based on GWAS of pre-anthesis phase duration in
1037 spring barley. PLoS One. 2014;9(11):e113120. doi: 10.1371/journal.pone.0113120.
1038 PMID: 25420105.
1039 39. Casto AL, Mattison AJ, Olson SN, Thakran M, Rooney WL, Mullet JE. *Maturity2*, a
1040 novel regulator of flowering time in *Sorghum bicolor*, increases expression of *SbPRR37*
1041 and *SbCO* in long days delaying flowering. PLoS One. 2019;14(4):e0212154. doi:
1042 10.1371/journal.pone.0212154. PMID: 30969968.
1043 40. Yang S, Murphy RL, Morishige DT, Klein PE, Rooney WL, Mullet JE. Sorghum
1044 phytochrome B inhibits flowering in long days by activating expression of *SbPRR37* and
1045 *SbGHD7*, repressors of *SbEHD1*, *SbCN8* and *SbCN12*. PLoS One. 2014;9(8):e105352.
1046 doi: 10.1371/journal.pone.0105352. PMID: 25122453.
1047 41. Yang S, Weers BD, Morishige DT, Mullet JE. *CONSTANS* is a photoperiod regulated
1048 activator of flowering in sorghum. BMC Plant Biol. 2014;14:148. doi: 10.1186/1471-
1049 2229-14-148. PMID: 24884377.
1050 42. Nemoto Y, Kisaka M, Fuse T, Yano M, Ogihara Y. Characterization and functional
1051 analysis of three wheat genes with homology to the *CONSTANS* flowering time gene in
1052 transgenic rice. Plant J. 2003;36(1):82-93. doi: 10.1046/j.1365-313x.2003.01859.x.
1053 PMID: 12974813.

1054 43. Woods DP, McKeown MA, Dong Y, Preston JC, Amasino RM. Evolution of
1055 *VRN2/Ghd7*-like genes in vernalization-mediated repression of grass flowering. Plant
1056 Physiol. 2016;170(4):2124-35. doi: 10.1104/pp.15.01279. PMID: 26848096.
1057 44. Fujino K, Yamanouchi U, Nonoue Y, Obara M, Yano M. Switching genetic effects of the
1058 flowering time gene *Hd*1 in LD conditions by *Ghd7* and *OsPRR37* in rice. Breeding Sci.
1059 2019;69(1):127-32. doi: 10.1270/jsbbs.18060. PMID: 31086490.
1060 45. Zhang Z, Hu W, Shen G, Liu H, Hu Y, Zhou X, et al. Alternative functions of Hd1 in
1061 repressing or promoting heading are determined by Ghd7 status under long-day
1062 conditions. Sci Rep-Uk. 2017;7(1):5388. doi: 10.1038/s41598-017-05873-1. PMID:
1063 28710485.
1064 46. Zhang B, Liu H, Qi F, Zhang Z, Li Q, Han Z, et al. Genetic interactions among *Ghd7*,
1065 *Ghd8*, *OsPRR37* and *Hd1* contribute to large variation in heading date in rice. Rice (N
1066 Y). 2019;12(1):48. doi: 10.1186/s12284-019-0314-x. PMID: 31309345.
1067 47. Maurer A, Draba V, Jiang Y, Schnaithmann F, Sharma R, Schumann E, et al. Modelling
1068 the genetic architecture of flowering time control in barley through nested association
1069 mapping. BMC Genomics. 2015;16:290. doi: 10.1186/s12864-015-1459-7. PMID:
1070 25887319.
1071 48. Shaw LM, Turner AS, Laurie DA. The impact of photoperiod insensitive *Ppd-1a*
1072 mutations on the photoperiod pathway across the three genomes of hexaploid wheat
1073 (*Triticum aestivum*). Plant J. 2012;71(1):71-84. doi: 10.1111/j.1365-313X.2012.04971.x.
1074 PMID: 22372488.

1075 49. Qin Z, Bai Y, Muhammad S, Wu X, Deng P, Wu J, et al. Divergent roles of *FT-like 9* in
1076 flowering transition under different day lengths in *Brachypodium distachyon*. Nat
1077 Commun. 2019;10(1):812. doi: 10.1038/s41467-019-08785-y. PMID: 30778068.
1078 50. Wang P, Gong R, Yang Y, Yu S. *Ghd8* controls rice photoperiod sensitivity by forming a
1079 complex that interacts with *Ghd7*. BMC Plant Biol. 2019;19(1):462. doi:
1080 10.1186/s12870-019-2053-y. PMID: 31675987.
1081 51. Yan L, Fu D, Li C, Blechl A, Tranquilli G, Bonafede M, et al. The wheat and barley
1082 vernalization gene *VRN3* is an orthologue of *FT*. Proc Natl Acad Sci U S A.
1083 2006;103(51):19581-6. doi: 10.1073/pnas.0607142103. PMID: 17158798.
1084 52. Deng W, Casao MC, Wang P, Sato K, Hayes PM, Finnegan EJ, et al. Direct links
1085 between the vernalization response and other key traits of cereal crops. Nat Commun.
1086 2015;6:5882. doi: 10.1038/ncomms6882. PMID: 25562483.
1087 53. Li C, Lin H, Dubcovsky J. Factorial combinations of protein interactions generate a
1088 multiplicity of florigen activation complexes in wheat and barley. Plant J. 2015;84:70-82.
1089 54. Turner AS, Faure S, Zhang Y, Laurie DA. The effect of day-neutral mutations in barley
1090 and wheat on the interaction between photoperiod and vernalization. Theor Appl Genet.
1091 2013;126(9):2267-77. doi: 10.1007/s00122-013-2133-6. PMID: 23737074.
1092 55. Hayama R, Sarid-Krebs L, Richter R, Fernandez V, Jang S, Coupland G. PSEUDO
1093 RESPONSE REGULATORs stabilize CONSTANS protein to promote flowering in
1094 response to day length. Embo J. 2017;36(7):904-18. doi: 10.15252/embj.201693907.
1095 PMID: 28270524.
1096 56. Nakamichi N, Kita M, Ito S, Yamashino T, Mizuno T. PSEUDO-RESPONSE
1097 REGULATORS, PRR9, PRR7 and PRR5, together play essential roles close to the

1098 circadian clock of *Arabidopsis thaliana*. Plant Cell Physiol. 2005;46(5):686-98. doi:
1099 10.1093/pcp/pci086. PMID: 15767265.
1100 57. Murakami M, Tago Y, Yamashino T, Mizuno T. Characterization of the rice circadian
1101 clock-associated pseudo-response regulators in *Arabidopsis thaliana*. Biosci Biotech
1102 Bioch. 2007;71(4):1107-10. doi: 10.1271/bbb.70048. PMID: 17420570.
1103 58. Campoli C, Shtaya M, Davis SJ, von Korff M. Expression conservation within the
1104 circadian clock of a monocot: natural variation at barley *Ppd-H1* affects circadian
1105 expression of flowering time genes, but not clock orthologs. BMC Plant Biol.
1106 2012;12:97. doi: 10.1186/1471-2229-12-97. PMID: 22720803.
1107 59. Ben-Naim O, Eshed R, Parnis A, Teper-Bamnolker P, Shalit A, Coupland G, et al. The
1108 CCAAT binding factor can mediate interactions between CONSTANS-like proteins and
1109 DNA. Plant J. 2006;46(3):462-76. doi: 10.1111/j.1365-313X.2006.02706.x. PMID:
1110 16623906.
1111 60. Kumimoto RW, Adam L, Hymus GJ, Repetti PP, Reuber TL, Marion CM, et al. The
1112 Nuclear Factor Y subunits NF-YB2 and NF-YB3 play additive roles in the promotion of
1113 flowering by inductive long-day photoperiods in Arabidopsis. Planta. 2008;228(5):709-
1114 23. doi: 10.1007/s00425-008-0773-6. PMID: 18600346.
1115 61. Wenkel S, Turck F, Singer K, Gissot L, Le Gourrierec J, Samach A, et al. CONSTANS
1116 and the CCAAT box binding complex share a functionally important domain and interact
1117 to regulate flowering of Arabidopsis. Plant Cell. 2006;18(11):2971-84. doi:
1118 10.1105/tpc.106.043299. PMID: 17138697.
1119 62. Woods DP, Ream TS, Minevich G, Hobert O, Amasino RM. PHYTOCHROME C is an
1120 essential light receptor for photoperiodic flowering in the temperate grass, *Brachypodium*

1121 *distachyon*. Genetics. 2014;198(1):397-408. doi: 10.1534/genetics.114.166785. PMID:
1122 25023399.
1123 63. Osugi A, Itoh H, Ikeda-Kawakatsu K, Takano M, Izawa T. Molecular dissection of the
1124 roles of phytochrome in photoperiodic flowering in rice. Plant Physiol.
1125 2011;157(3):1128-37. doi: 10.1104/pp.111.181792. PMID: 21880933.
1126 64. Zheng T, Sun J, Zhou S, Chen S, Lu J, Cui S, et al. Post-transcriptional regulation of
1127 Ghd7 protein stability by phytochrome and OsGI in photoperiodic control of flowering in
1128 rice. New Phytol. 2019;224(1):306-20. doi: 10.1111/nph.16010. PMID: 31225911.
1129 65. Valverde F, Mouradov A, Soppe W, Ravenscroft D, Samach A, Coupland G.
1130 Photoreceptor regulation of CONSTANS protein in photoperiodic flowering. Science.
1131 2004;303(5660):1003-6. doi: 10.1126/science.1091761. PMID: 14963328.
1132 66. Hayama R, Coupland G. The molecular basis of diversity in the photoperiodic flowering
1133 responses of Arabidopsis and rice. Plant Physiol. 2004;135(2):677-84. doi: DOI
1134 10.1104/pp.104.042614. PMID: ISI:000222165300012.
1135 67. Krasileva KV, Buffalo V, Bailey P, Pearce S, Ayling S, Tabbita F, et al. Separating
1136 homeologs by phasing in the tetraploid wheat transcriptome. Genome Biol.
1137 2013;14(6):R66. doi: 10.1186/gb-2013-14-6-r66. PMID: 23800085.
1138 68. Shan Q, Wang Y, Li J, Gao C. Genome editing in rice and wheat using the CRISPR/Cas
1139 system. Nat Protoc. 2014;9(10):2395-410. doi: 10.1038/nprot.2014.157. PMID:
1140 25232936.
1141
1142
1143

1144 **SUPPORTING INFORMATION CAPTIONS**

1145 **Supplementary Fig S1.** Shoot apical meristem (SAM) and spike development.

1146 **Supplementary Fig S2.** Dissection of developing spikes.

1147 **Supplementary Fig S3.** Effect of *ppd1*, *co1* and *co2* loss-of-function mutations and photoperiod

1148 on *CO1* and *CO2* transcript levels.

1149 **Supplementary Fig S4.** Effect of *phyB*-null and *phyC*-null mutations in Kronos-PI on the

1150 transcriptional profiles of *CO1* and *CO2* under SD and LD.

1151 **Supplementary Fig S5.** Yeast-two-hybrid (Y2H) assays.

1152 **Supplementary Table S1.** Genome-specific primer sequences and PCR conditions for

1153 TILLING.

1154 **Supplementary Table S2.** Number of mutations detected in the targeted regions of wheat *CO1*

1155 and *CO2* homologs in the Kronos TILLING population.

1156 **Table S3**. Analysis of variance for heading time under long days.

1157 **Table S4**. Analysis of variance for heading time under short days.

1158 **Table S5**. Primers used in the qRT-PCR and Y2H experiments.